Heat stored in the Earth system: Where does the energy go?
The GCOS Earth heat inventory team

Karina von Schuckmann[1], Lijing Cheng[2,28], Matthew D. Palmer[3], James Hansen[4], Caterina Tassone[5], Valentin Aich[5], Susheel Adusumilli[6], Hugo Beltrami[7], Tim Boyer[8], Francisco José Cuesta-Valero[7,27], Damien Desbruyères[9], Catia Domingues[10,11], Almudena García-García[7], Pierre Gentine[12], John Gilson[13], Maximilian Gorfer[14], Leopold Haimberger[15], Masayoshi Ishii[16], Gregory C. Johnson[17], Rachel Killick[3], Brian A. King[10], Gottfried Kirchengast[14], Nicolas Kolodziejczyk[18], John Lyman[17], Ben Marzeion[19], Michael Mayer[15,29], Maeva Monier[20], Didier Paolo Monselesan[21], Sarah Purkey[6], Dean Roemmich[6], Axel Schweiger[22], Sonia I. Seneviratne[23], Andrew Shepherd[24], Donald A. Slater[6], Andrea K. Steiner[14], Fiammetta Straneo[6], Mary-Louise Timmermans[25], Susan E. Wijffels[21,26]

[1]Mercator Ocean International, France
[2]Institute of Atmospheric Physics, Chinese Academy of Sciences, China
[3]Met Office Hadley Centre, UK
[4]Columbia University Earth Institute, USA
[5]WMO/GCOS, Switzerland
[6]Scripps Institution of Oceanography, UCSD, San Diego, CA, USA
[7]Climate & Atmospheric Sciences Institute, St. Francis Xavier University, NS, Canada
[8]NOAA's National Centers for Environmental Information
[9]Ifremer, University of Brest, CNRS, IRD, Laboratoire d'Océanographie Physique et Spatiale, France
[10]National Oceanographic Centre, UK
[11]ARC Centre of Excellence for Climate Extremes, University of Tasmania, Hobart, Tasmania, Australia
[12]Earth and Environmental Engineering in the School of Engineering and Applied Sciences, Columbia University, USA
[13]University of California, USA
[14]Wegener Center for Climate and Global Change and Institute of Physics, University of Graz, Austria
[15]Department of Meteorology and Geophysics, University of Vienna, Austria
[16]Department of Atmosphere, Ocean and Earth System Modeling Research, Meteorological Research Institute, Japan
[17]NOAA, Pacific Marine Environmental Laboratory, USA
[18]University of Brest, CNRS, IRD, Ifremer, Laboratoire d'Océanographie Physique et Spatiale, IUEM, France
[19]Institute of Geography and MARUM-Center for Marine Environmental Sciences, University of Bremen, Germany
[20]CELAD/Mercator Ocean International, France
[21]CSIRO Oceans and Atmosphere, Hobart, Tasmania, Australia
[22]Polar Science Center, Applied Physics Laboratory, University of Washington, Seattle, USA
[23]Institute for Atmospheric and Climate Science, ETH, Switzerland
[24]Center for Polar Observation and Modeling, University of Leeds, UK
[25]Department of Earth and Planetary Sciences, Yale University, New Haven, USA
[26]Woods Hole Oceanographic Institution, Massachusetts, United States
[27]Environmental Sciences Program, Memorial University of Newfoundland, NL, Canada
[28]Center for Ocean Mega-Science, Chinese Academy of Sciences, Qingdao, China, 266071
[29]European Centre for Medium-Range Weather Forecasts, Reading, UK

Correspondence to: Karina von Schuckmann (karina.von.schuckmann@mercator-ocean.fr)

Abstract

48

Human-induced atmospheric composition changes cause a radiative imbalance at the top-of-atmosphere which is driving global warming. This Earth Energy Imbalance (EEI) is the most critical number defining the prospects for continued global warming and climate change. Understanding the heat gain of the Earth system – and particularly how much and where the heat is distributed – is fundamental to understanding how this affects warming ocean, atmosphere, and land; rising surface temperature; sea level; and loss of grounded and floating ice, which are fundamental concerns for society. This study is a Global Climate Observing System (GCOS) concerted international effort to update the Earth heat inventory, and presents an updated assessment of ocean warming estimates, and new and updated estimates of heat gain in the atmosphere, cryosphere and land over the period 1960-2018. The study obtains a consistent long-term Earth system heat gain over the period 1971-2018, with a total heat gain of 358 ± 37 ZJ, which is equivalent to a global heating rate of 0.47 ± 0.1 W/m^2. Over the period 1971-2018 (2010-2018), the majority of heat gain is reported for the global ocean with 89% (90%), with 52% for both periods in the upper 700m depth, 28% (30%) for the 700-2000m depth layer, and 9% (8%) below 2000m depth. Heat gain over land amounts to 6% (5%) over these periods, 4% (3%) is available for the melting of grounded and floating ice, and 1% (2%) for atmospheric warming. Our results also show that EEI is not only continuing, it is increasing: the EEI amounts to 0.87 ± 0.12 W/m^2 during 2010-2018. Stabilization of climate, the goal of the universally agreed UNFCCC in 1992 and the Paris agreement in 2015, requires that EEI be reduced to approximately zero to achieve Earth's system quasi-equilibrium. The amount of CO_2 in the atmosphere would need to be reduced from 410 ppm to 353 ppm to increase heat radiation to space by 0.87 W/m^2, bringing Earth back towards energy balance. This simple number, EEI, is the most fundamental metric that the scientific community and public must be aware of, as the measure of how well the world is doing in the task of bringing climate change under control, and we call for an implementation of the EEI into the global stocktake based on best available science. Continued quantification and reduced uncertainties in the Earth heat inventory can be best achieved through the maintenance of the current global climate observing system, its extension into areas of gaps in the sampling, as well as to establish an international framework for concerted multi-disciplinary research of the Earth heat inventory as presented in this study. This Earth heat inventory is published at DKRZ (https://www.dkrz.de/) under the doi: https://doi.org/10.26050/WDCC/GCOS_EHI_EXP_v2 (von Schuckmann et al., 2020).

80

81

82

83

84

Introduction

In the Paris Agreement of the United Nations Framework Convention on Climate Change (UNFCCC), article 7 demands that "Parties should strengthen […] scientific knowledge on climate, including research, systematic observation of the climate system and early warning systems, in a manner that informs climate services and supports decision-making." This request of the UNFCCC expresses the need of climate monitoring based on best available science, which is globally coordinated through the Global Climate Observing System (GCOS). In the current Implementation Plan of GCOS, main observation gaps are addressed and it states that "closing the Earth's energy balance […] through observations remain outstanding scientific issues that require high-quality climate records of Essential Climate Variables (ECVs)." (GCOS, 2016). GCOS is asking the broader scientific community to establish the observational requirements needed to meet the targets defined in the GCOS Implementation Plan, and to identify how climate observations could be enhanced and continued into the future in order to monitor the Earth's cycles and the global energy budget. This study addresses and intends to respond to this request.

The state, variability and change of Earth's climate are to a large extent driven by the energy transfer between the different components of the Earth system (Hansen, 2005; Hansen et al., 2011). Energy flows alter clouds, and weather and internal climate modes can temporarily alter the energy balance on sub-annual to multi-decadal timescales (Palmer & McNeall, 2014; Rhein et al., 2013). The most practical way to monitor climate state, variability and change is to continually assess the energy, mainly in the form of heat, in the Earth system (Hansen et al., 2011). All energy entering or leaving the Earth climate system does so in the form of radiation at the top-of-the-atmosphere (TOA) (Loeb et al., 2012). The difference between incoming solar radiation and outgoing radiation, which is the sum of the reflected shortwave radiation and emitted longwave radiation, determines the net radiative flux at TOA. Changes of this global radiation balance at TOA - the so-called Earth Energy Imbalance (EEI) - determines the temporal evolution of Earth's climate: If the imbalance is positive (i.e. less energy going out than coming in), energy in the form of heat is accumulated in the Earth system resulting in global warming - or cooling if the EEI is negative. The various facets and impacts of observed climate change arise due to the EEI, which thus represents a crucial measure of the rate of climate change (von Schuckmann et al., 2016). The EEI is the portion of the forcing that has not yet been responded to (Hansen, 2005). In other words, warming will continue even if atmospheric greenhouse gas (GHG) amounts are stabilized at today's level, and the EEI defines additional global warming that will occur without further change in forcing (Hansen et al., 2017). The EEI is less subject to decadal variations associated with internal climate variability than global surface temperature and therefore represents a robust measure of the rate of climate change (von Schuckmann et al., 2016; Cheng et al., 2017).

The Earth system responds to an imposed radiative forcing through a number of feedbacks, which operate on various different timescales. Conceptually, the relationships between EEI, radiative forcing, and surface temperature change can be expressed as (Gregory & Andrews, 2016):

$$\Delta N_{TOA} = \Delta F_{ERF} - |\alpha_{FP}| \Delta T_S \qquad (1)$$

127

128   where ΔN_{TOA} is Earth's net energy imbalance at the Top of the Atmosphere (TOA, in W m^{-2}),
129   ΔF_{ERF} is the effective radiative forcing (W m^{-2}), ΔT_S is the global surface temperature anomaly
130   (K) relative to the equilibrium state, and α_{FP} is the net total feedback parameter (W m^{-2} K^{-1}), which
131   represents the combined effect of the various climate feedbacks. Essentially, α_{FP} in Equ. (1) can
132   be viewed as a measure of how efficient the system is at restoring radiative equilibrium for a unit
133   surface temperature rise. Thus, ΔN_{TOA} represents the difference between the applied radiative
134   forcing and Earth's radiative response through climate feedbacks associated with surface
135   temperature rise (e.g. Hansen et al., 2011). Observation-based estimates of ΔN_{TOA} are therefore
136   crucial both to our understanding of past climate change and for refining projections of future
137   climate change (Gregory & Andrews, 2016; Kuhlbrodt & Gregory, 2012). The long atmospheric
138   lifetime of carbon dioxide means that $\Delta N_{TOA},$ ΔF_{ERF} and ΔT_S will remain positive for centuries,
139   even with substantial reductions in greenhouse gas emissions and lead to substantial committed
140   sea-level rise (Cheng, Abraham, et al., 2019; Hansen et al., 2017; Nauels et al., 2017; Matthew D
141   Palmer et al., 2018).

142

143   However, this conceptual picture is complicated by the presence of unforced internal variability in
144   the climate system, which adds substantial noise to the real-world expression of this equation
145   (Gregory et al., 2020; Marvel et al., 2018; Palmer & McNeall, 2014). For example, at time scales
146   from interannual to decadal periods, the phase of the El Niño Southern Oscillation contributes to
147   both positive or negative variations in EEI (Cheng, Trenberth, et al., 2019; Loeb et al., 2018;
148   Johnson and Birnbaum, 2017; Loeb et al., 2012). At multi-decadal and longer time scales,
149   systematic changes in ocean circulation can significantly alter the EEI as well (Baggenstos et al.,
150   2019).

151

152   Time-scales of the Earth climate response to perturbations of the equilibrium Earth energy balance
153   at TOA are driven by a combination of climate forcing and the planet's thermal inertia: The Earth
154   system tries to restore radiative equilibrium through increased thermal radiation to space via the
155   Planck response, but a number of additional Earth system feedbacks also influence the planetary
156   radiative response (Lembo et al., 2019; Myhre et al., 2013). Time-scales of warming or cooling of
157   the climate depend on the imposed radiative forcing, the evolution of climate and Earth system
158   feedbacks with ocean and cryosphere in particular leading to substantial "thermal inertia" (Clark
159   et al., 2016; Marshall et al., 2015). Consequently, it requires centuries for Earth's surface
160   temperature to respond fully to a climate forcing.

161

162   Contemporary estimates of the magnitude of the Earth's energy imbalance range between about
163   0.4-0.9 W m^{-2} (depending on estimate method and period, see also conclusion), and are directly
164   attributable to increases in carbon dioxide and other greenhouse gases in the atmosphere from
165   human activities (Ciais et al., 2013, Myhre et al., 2013, Rhein et al., 2013, Hansen et al., 2011).
166   The estimate obtained from climate models (CMIP6) as presented by (Wild, 2020) amounts to 1.1

167 ± 0.8 W m^{-2}. Since the period of industrialization, the EEI has become increasingly dominated by
168 the emissions of radiatively active greenhouse gases, which perturb the planetary radiation budget
169 and result in a positive EEI. As a consequence, excess heat is accumulated in the Earth system,
170 which is driving global warming (Hansen et al., 2005; 2011). The majority (about 90%) of this
171 positive EEI is stored in the ocean (Rhein et al., 2013) and can be estimated through the evaluation
172 of ocean heat content (OHC, e.g. Abraham et al., 2013). According to previous estimates, a small
173 proportion (~3%) contributes to the melting of Arctic sea ice and land ice (glaciers, the Greenland
174 and Antarctic ice sheets). Another 4% goes into heating of the land and atmosphere (Rhein et al.,
175 2013).

176

177 Knowing where and how much heat is stored in the different Earth system components from a
178 positive EEI, and quantifying the Earth heat inventory is of fundamental importance to unravel the
179 current status of climate change, as well as to better understand and predict its implications, and
180 to design the optimal observing networks for monitoring the Earth heat inventory. Quantifying this
181 energy gain is essential for understanding the response of the climate system to radiative forcing,
182 and hence to reduce uncertainties in climate predictions. The rate of ocean heat gain is a key
183 component for the quantification of the EEI, and the observed surface warming has been used to
184 estimate the equilibrium climate sensitivity (e.g. Knutti & Rugenstein, 2015). However, further
185 insight into the Earth heat inventory, particularly to further unravel on where the heat is going, can
186 have implications on the understanding of the transient climate responses to climate change, and
187 consequently reduces uncertainties in climate predictions (Hansen et al., 2011). In this paper, we
188 focus on the inventory of heat stored in the Earth system. The first four sections will introduce the
189 current status of estimate of heat storage change in the ocean, atmosphere, land and cryosphere,
190 respectively. Uncertainties, current achieved accuracy, challenges, and recommendations for
191 future improved estimates are discussed for each Earth system component, and in the conclusion.
192 In the last chapter, an update of the Earth heat inventory is established based on the results of
193 sections 1-4, followed by a conclusion.

194

195

196 ## 1. Heat stored in the ocean

197

198 The storage of heat in the ocean leads to ocean warming (IPCC, 2019), and is a major contributor
199 to sea-level rise through thermal expansion (WCRP, 2018). Ocean warming alters ocean
200 stratification and ocean mixing processes (Bindoff et al., 2019), affects ocean currents (Hoegh-
201 Guldberg, 2018; Monika Rhein et al., 2018; Yang et al., 2016), impacts tropical cyclones (Hoegh-
202 Guldberg, 2018; Trenberth et al., 2018; Woollings et al., 2012) and is a major player in ocean
203 deoxygenation processes (Breitburg et al., 2018) and carbon sequestration into the ocean (Bopp et
204 al., 2013; Frölicher et al., 2018). Together with ocean acidification and deoxygenation, ocean
205 warming can lead to dramatic changes in ecosystems, biodiversity, population extinctions, coral
206 bleaching and infectious disease, as well as redistribution of habitat (García Molinos et al., 2016;

Gattuso et al., 2015; Ramírez et al., 2017). Implications of ocean warming are also widespread across Earth's cryosphere (Jacobs et al., 2002; Mayer et al., 2019; Polyakov et al., 2017; Serreze & Barry, 2011; Shi et al., 2018). Examples include the basal melt of ice shelves (Adusumilli et al., 2019; Pritchard et al., 2012; Wilson et al., 2017) and marine terminating glaciers (Straneo & Cenedese, 2015); the retreat and speedup of outlet glaciers in Greenland (King et al., 2018) and in Antarctica (Shepherd, Fricker, et al., 2018) and of tidewater glaciers in South America and in the High Arctic (Gardner et al., 2013).

Opportunities and challenges in forming OHC estimates depend on the availability of in situ subsurface temperature measurements, particularly for global-scale evaluations. Subsurface ocean temperature measurements before 1900 had been obtained from ship-board instrumentation, culminating in the global-scale Challenger expedition (1873–1876) (Roemmich & Gilson, 2009). From 1900 up to the mid-1960s, subsurface temperature measurements relied on ship-board Nansen-Bottle and mechanical bathythermograph (MBT) instruments (Abraham et al., 2013), only allowing limited global coverage and data quality. The inventions of the conductivity-temperature-depth (CTD) instruments in the mid-50s and the Expendable Bathythermograph Observing (XBT) system about ten years later increased the oceanographic capabilities for widespread and accurate (in the case of the CTD) measurements of in situ subsurface water temperature (Abraham et al., 2013; Goni et al., 2019).

With the implementation of several national and international programs, and the implementation of the moored arrays in the tropical ocean in the 1980s, the Global Ocean Observing System (GOOS, https://www.goosocean.org/) started to grow. Particularly the global World Ocean Circulation program (WOCE) during the 1990s obtained a global baseline survey of the ocean from top-to-bottom (King et al., 2001). However, measurements were still limited to fixed point platforms, major shipping routes and Naval and research vessel cruise tracks, leaving large parts of the ocean under-sampled. In addition, detected instrumental biases in MBTs, XBTs and other instruments pose a further challenge for the global scale OHC estimate (Abraham et al., 2013; Ciais et al., 2013; M. Rhein et al., 2013), but significant progress has been made recently to correct biases and provide high-quality data for climate research (Boyer et al., 2016; Cheng et al., 2016; Goni et al., 2019; Gouretski & Cheng, 2020). Satellite altimeter measurements of sea surface height began in 1992, and are used to complement in situ derived OHC estimates, either for validation purposes (Cabanes et al., 2013), or to complement the development of global gridded ocean temperature fields (Guinehut et al., 2012; Willis et al., 2004). Indirect estimates of OHC from remote sensing through the global sea level budget became possible with satellite-derived ocean mass information in 2002 (Dieng et al., 2017; Llovel et al., 2014; Loeb et al., 2012; Meyssignac et al., 2019; von Schuckmann et al., 2014).

After the Oceanobs conference in 1999, the international Argo profiling float program was launched with first Argo float deployments in the same year (Riser et al., 2016; Roemmich &

Gilson, 2009). By the end of 2006, Argo sampling had reached its initial target of data sampling roughly every 3 degrees between 60°S-60°N. However, due to technical evolution, only 40% of Argo floats provided measurements down to 2000 m depth in the year 2005, but that percentage increased to 60% in 2010 (von Schuckmann & Le Traon, 2011). The starting point of Argo-based 'best estimate' for near-global-scale (60°S-60°N) OHC is either defined in 2005 (von Schuckmann and Le Traon, 2011), or in 2006 (Wijffels et al., 2016). The opportunity for improved OHC estimation provided by Argo is tremendous, and has led to major advancements in climate science, particularly on the discussion of the EEI (Hansen et al., 2011; Johnson, et al., 2018; Loeb et al., 2012; Trenberth & Fasullo, 2010; von Schuckmann et al., 2016, Meyssignac et al., 2019). The near-global coverage of the Argo network also provides an excellent test bed for the long-term OHC reconstruction extending back well before the Argo period (Cheng et al., 2017). Moreover, these evaluations inform further observing system recommendations for global climate studies, i.e. gaps in the deep ocean layers below 2000m depth, in marginal seas, in shelf areas and in the polar regions (e.g. von Schuckmann et al., 2016), and their implementations are underway, for example for deep Argo (Johnson et al., 2019).

Different research groups have developed gridded products of subsurface temperature fields for the global ocean using statistical models (Gaillard et al., 2016; Good et al., 2013; Ishii et al., 2017; Levitus et al., 2012) or combined observations with additional statistics from climate models (Cheng et al., 2017). An exhaustive list of the pre-Argo products can be found in for example Abraham et al., 2013; Boyer et al., 2016; WCRP, 2018; Meyssignac et al., 2019. Additionally, specific Argo-based products are listed on the Argo webpage (http://www.argo.ucsd.edu/). Although all products rely more or less on the same database, near-global OHC estimates show some discrepancies which result from the different statistical treatments of data gaps, the choice of the climatology and the approach used to account for the MBT and XBT instrumental biases (Boyer et al., 2016; Wang et al., 2018). Argo-based products show smaller differences, likely resulting from different treatments of currently under-sampled regions (e.g. von Schuckmann et al., 2016). Ocean reanalysis systems have been also used to deliver estimates of near-global OHC (Meyssignac et al., 2019; von Schuckmann et al., 2018), and their international assessments show increased discrepancies with decreasing in situ data availability for the assimilation (Palmer et al., 2017; Storto et al., 2018). Climate models have also been used to study global and regional ocean heat changes and the associated mechanisms, with observational datasets providing valuable benchmarks for model evaluation (Cheng et al., 2016; Gleckler et al., 2016).

International near-global OHC assessments have been performed previously (e.g. Abraham et al., 2013; Boyer et al., 2016; Meyssignac et al., 2019; WCRP, 2018). These assessments are challenging, as most of the gridded temperature fields are research products, and only few are distributed and regularly updated operationally (e.g. https://marine.copernicus.eu/). This initiative relies on the availability of data products, their temporal extensions, and direct interactions with the different research groups. A complete view of all international temperature products can be

287 only achieved through a concerted international effort, and over time. In this study, we do not
288 achieve a holistic view of all available products, but present a starting point for future international
289 regular assessments of near-global OHC. For the first time, we propose an international ensemble
290 mean and standard deviation of near-global OHC (Fig. 1) which is then used to build an Earth
291 climate system energy inventory (section 5). The ensemble spread gives an indication of the
292 agreement among products and can be used as a proxy for uncertainty. The basic assumption for
293 the error distribution is Gaussian with a mean of zero, which can be approximated by an ensemble
294 of various products. However, it does not account for systematic errors that may result in biases
295 across the ensemble and does not represent the full uncertainty. The uncertainty can also be
296 estimated in other ways including some purely statistical methods (Levitus et al., 2012) or methods
297 explicitly accounting for the error sources (Lyman & Johnson, 2013), but each method has its
298 caveats, for example the error covariances are mostly unknown, so adopting a straightforward
299 method with a "data democracy" strategy has been chosen here as a starting point.

300

301 However, future evolution of this initiative is needed to include missing and updated in situ-based
302 products, ocean reanalyses, as well as indirect estimates (for example satellite-based). The
303 continuity of this activity will help to further unravel uncertainties due to the community's
304 collective efforts on detecting/reducing errors, and then provides up-to-date scientific knowledge
305 of ocean heat uptake.

306

307
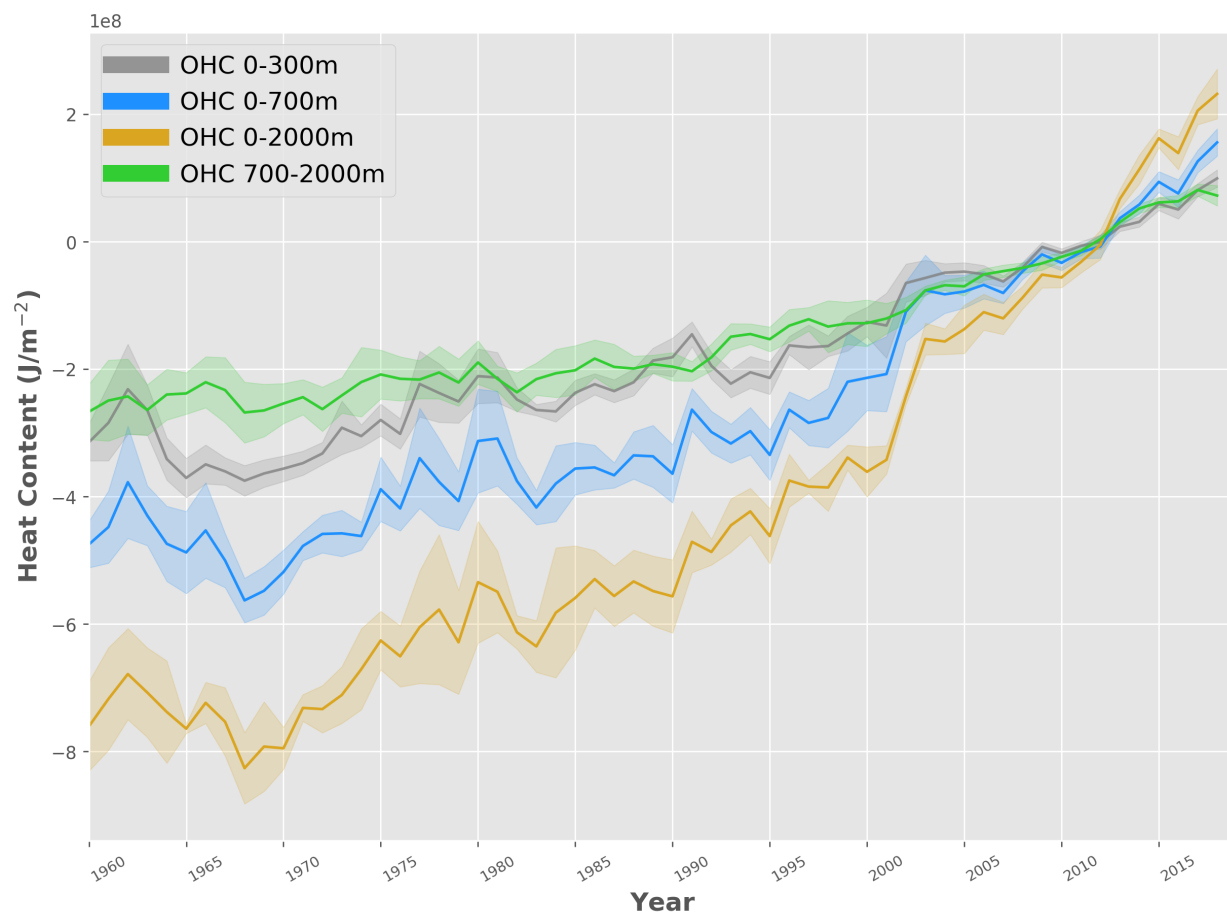
308
309 ***Figure 1:*** *Ensemble mean time series and ensemble standard deviation (2-sigma, shaded) of global ocean*
310 *heat content (OHC) anomalies relative to the 2005-2017 climatology for the 0-300m (grey), 0-700m (blue),*
311 *0-2000m (yellow) and 700-2000m depth layer (green). The ensemble mean is an outcome of an*
312 *international assessment initiative, and all products used are referenced in the legend of Fig. 2. The trends*
313 *derived from the time series are given in Table 1. Note that values are given for the ocean surface area*
314 *between 60°S-60°N, and limited to the 300m bathymetry of each product, respectively.*
315
316

Period	0-300m (W/m²)	0-700m (W/m²)	0-2000m (W/m²)	700-2000m (W/m²)
1960-2018	0.3 ± 0.03	0.4 ± 0.1	0.5 ± 0.1	0.2 ± 0.03
1993-2018	0.4 ± 0.04	0.6 ± 0.1	0.9 ± 0.1	0.3 ± 0.03
2005-2018	0.4 ± 0.1	0.6 ± 0.1	1.0 ± 0.2	0.4 ± 0.1
2010-2018	0.5 ± 0.1	0.7 ± 0.1	1.3 ± 0.3	0.5 ± 0.1

Table 1: Linear trends (weighted least square fit, see for example von Schuckmann and Le Traon, 2011) as derived from the ensemble mean as presented in Fig. 1 for different time intervals, and different integration depth. The uncertainty on the trend estimate is given for the 95% confidence level. Note that values are given for the ocean surface area between 60°S-60°N, and limited to the 300m bathymetry of each product, respectively. See text and Fig. 1 caption for more details on the OHC estimates.

Products used for this assessment are referenced in the caption of Fig. 2. Estimates of OHC have been provided by the different research groups under homogeneous criteria. All estimates use a coherent ocean volume limited by the 300m isobath of each product, and are limited to 60°S-60°N since most observational products exclude high latitude ocean areas because of the low observational coverage, and only annual averages have been used. 60°S-60°N constitutes ~91% of the global ocean surface area and limiting to 300m isobath neglects the contributions from coastal and shallow waters, so the resultant OHC trends will be underestimated if these ocean regions are warming. For example, neglecting shallow waters can account for 5-10% for 0-2000m OHC trends (von Schuckmann et al., 2014). A first initial test using Cheng et al., (2017) data indicates that OHC 0-2000m trends can be underestimated by ~10% if the ocean warming in the area polewards of 60° latitude is not taken into account (not shown). This is a caveat of the assessment in this review and will be addressed in the future.

The assessment is based on three distinct periods to account for the evolution of the observing system, i.e. 1960-2018 (i.e. 'historical'), 1993-2018 (i.e. 'altimeter era') and 2005-2018 (i.e. 'golden Argo-era'). In addition, ocean warming rates over the past decade are specifically discussed according to an apparent acceleration of global surface warming since 2010 (WMO, 2020; Blunden and Arndt, 2019). All time series reach the end in 2018 – which was one of the principal limitations for the inclusion of some products. Our final estimates of OHC for the upper 2000m over different periods are the ensemble average of all products, with the uncertainty range defined by the standard deviation (2-sigma) of the corresponding estimates used (Fig. 1).

346
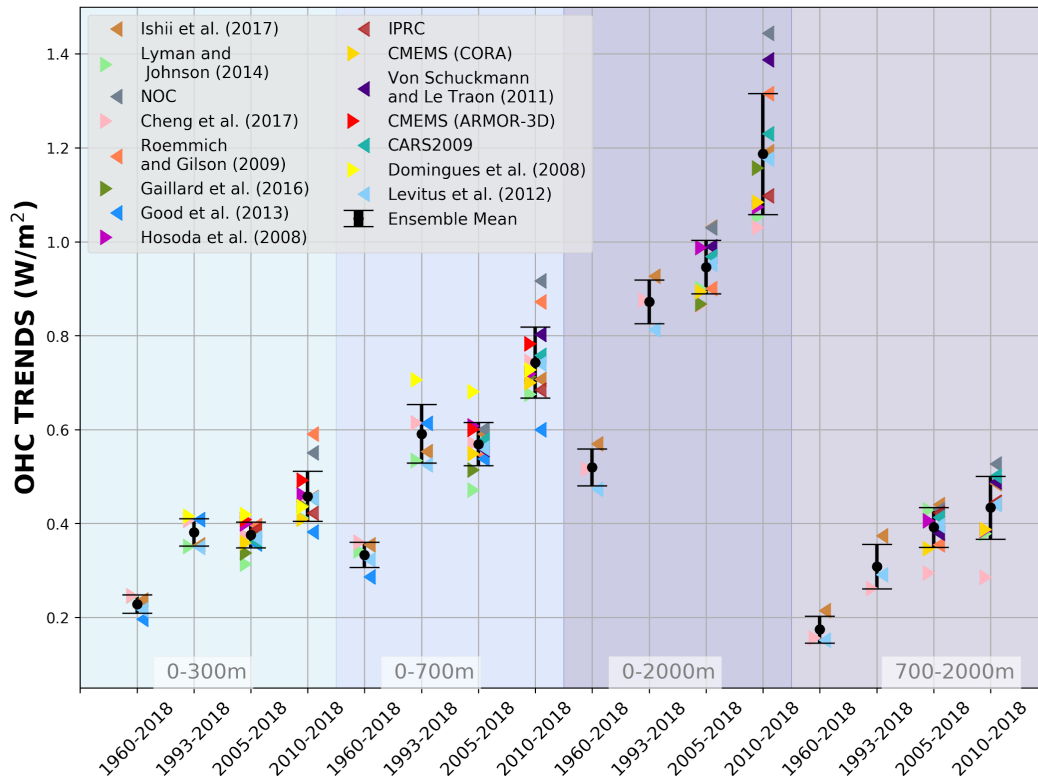
Figure 2: *Linear trends of global ocean heat content (OHC) as derived from different temperature products (colors). References are given in the figure legend, except for IPRC (http://apdrc.soest.hawaii.edu/projects/Argo/), CMEMS (CORA & ARMOR-3D, http://marine.copernicus.eu/science-learning/ocean-monitoring-indicators), CARS2009 (http://www.marine.csiro.au/~dunn/cars2009/) and NOC (National Oceanographic Institution,* (D. G. Desbruyères et al., 2016)*. The ensemble mean and standard deviation (2-sigma) is given in black, respectively. The shaded areas show trends from different depth layer integrations, i.e. 0-300m (light turquoise), 0-700m (light blue), 0-2000m (purple) and 700-2000m (light purple). For each integration depth layer, trends are evaluated over the three study periods, i.e. historical (1960-2018), altimeter era (1993-2018) and golden Argo era (2005-2018). In addition, the most recent period 2010-2018 is included. See text for more details on the international assessment criteria. Note that values are given for the ocean surface area (see text for more details).*

The first and principal result of the assessment (Fig. 1) is an overall increase of the trend for the more recent two study periods e.g., the altimeter era (1993-2018) and golden Argo era (2005-2018) relative to the historical era (1960-2018), which is in agreement with previous results (e.g. Abraham et al., 2013). The trend values are all given in Table 1. A major part of heat is stored in the upper layers of the ocean (0-300m and 0-700m depth). However, heat storage at intermediate depth (700-2000m) increases at a comparable rate as reported for the 0-300m depth layer (Table

1, Fig. 2). There is a general agreement among the 15 international OHC estimates (Fig. 2). However, for some periods and depth layers the standard deviation reaches maximal values up to about 0.3 W/m^2. All products agree on the fact that ocean warming rates have increased in the past decades, and doubled since the beginning of the altimeter era (1993-2018 compared with 1960-2018) (Fig. 2). Moreover, there is a clear indication that heat sequestration into the deeper ocean layers below 700m depth took place over the past 6 decades linked to an increase of OHC trends over time (Fig. 2). In agreement with observed accelerated Earth surface warming over the past decade (WMO, 2020; Blunden and Arndt, 2019), ocean warming rates for the 0-2000m depth layer also reached record rates of 1.3 (0.9) ± 0.3 W/m^2 for the ocean (global) area over the period 2010-2018.

For the deep OHC changes below 2000m, we adapted an updated estimate from (Purkey & Johnson, 2010) (PG10) from 1991 to 2018, which is a constant linear trend estimate (1.15 +/- 0.57 ZJ/year, 0.07 ± 0.04 W/m^2). Some recent studies strengthened the results in PG10 (D. G. Desbruyères et al., 2016; Zanna et al., 2019). Desbruyères et al., (2016) examined the decadal change of the deep and abyssal OHC trends below 2000m in 1990s and 2000s, suggesting that there has not been a significant change in the rate of decadal global deep/abyssal warming from the 1990's to the 2000's and the overall deep ocean warming rate is consistent with PG10. Using a Green Function method, Zanna et al. (2019) reported a deep ocean warming rate of ~0.06 Wm^{-2} during the 2000s, consistent with PG10 used in this study. Zanna et al. (2019) shows a fairly weak global trend during the 1990s, inconsistent with observation-based estimates. This mismatch might come from the simplified or misrepresentation of surface-deep connections using ECCO reanalysis data and the use of time-mean Green's functions in Zanna et al. (2019), as well as from the limited spatial resolution of the observational network for relatively short time-spans. Furthermore, combining hydrographic and deep-Argo floats, a recent study (Johnson et al., 2019) reported an accelerated warming in the South Pacific Ocean in recent years, but a global estimate of the OHC rate of change over time is not available yet.

Before 1990, we assume zero OHC trend below 2000m, following the methodology in IPCC-AR5 (Rhein et al., 2013). The zero-trend assumption is made mainly because there are too few observations before 1990 to make an estimate of OHC change below 2000m. But it is a reasonable assumption because OHC 700-2000m warming was fairly weak before 1990 and heat might not have penetrated down to 2000m (Cheng et al., 2017). Zanna et al. (2019) also shows a near zero OHC trend below 2000m from the 1960s to 1980s. The derived time series is used for the Earth energy inventory in section 5. A centralized (around the year 2006) uncertainty approach has been applied for the deep (> 2000m depth) OHC estimate following the method of Cheng et al., (2017), which allows to extract an uncertainty range over the period 1993-2018 within the given [lower (1.15 -0.57 ZJ/year), upper (1.15 + 0.57 ZJ/year)] range of the deep OHC trend estimate. We then extend the obtained uncertainty estimate back from 1993 to 1960, with 0 OHC anomaly.

2. Heat available to warm the atmosphere

While the amount of heat accumulated in the atmosphere is small compared to the ocean, warming of the Earth's near-surface air and atmosphere aloft is a very prominent effect of climate change, which directly affects society. Atmospheric observations clearly reveal a warming of the troposphere over the last decades (Santer et al., 2017; Steiner et al., 2020) and changes in the seasonal cycle (Santer et al., 2018). Changes in atmospheric circulation (Cohen et al., 2014; Fu et al., 2019) together with thermodynamic changes (Fischer & Knutti, 2016; Trenberth et al., 2015) will lead to more extreme weather events and increase high impact risks for society (Coumou et al., 2018; Zscheischler et al., 2018). Therefore, a rigorous assessment of the atmospheric heat content in context with all Earth's climate subsystems is important for a full view on the changing climate system.

The atmosphere transports vast amounts of energy laterally and strong vertical heat fluxes occur at the atmosphere's lower boundary. The pronounced energy and mass exchanges within the atmosphere and with all other climate components is a fundamental element of Earth's climate (Peixoto & Oort, 1992). In contrast, long-term heat accumulation in the atmosphere is limited by its small heat capacity as the gaseous component of the Earth system (von Schuckmann et al., 2016).

Recent work revealed inconsistencies in earlier formulations of the atmospheric energy budget (Mayer et al., 2017; Trenberth & Fasullo, 2018), and hence a short discussion of the updated formulation is provided here. In a globally averaged and vertically integrated sense, heat accumulation in the atmosphere arises from a small imbalance between net energy fluxes at the top of the atmosphere (TOA) and the surface (denoted s). The heat budget of the vertically integrated and globally averaged atmosphere (indicated by the global averaging operator $\langle . \rangle$) reads as follows (Mayer et al., 2017):

$$\langle \frac{\partial AE}{\partial t} \rangle = \langle N_{TOA} \rangle - \langle F_s \rangle - \langle F_{snow} \rangle - \langle F_{PE} \rangle, \quad (2)$$

where, in mean-sea-level altitude (z) coordinates used here for integrating over observational data, the vertically integrated atmospheric energy content AE per unit surface area [Jm^{-2}] reads

$$AE = \int_{z_s}^{z_{TOA}} \rho (c_v T + g(z - z_s) + L_e q + \frac{1}{2} V^2) \, dz. \quad (3)$$

In Equation 2, AE represents the total atmospheric energy content, N_{TOA} the net radiation at top-of-the atmosphere, F_s net surface energy flux defined as the sum of net surface radiation and latent and sensible heat flux, and F_{snow} the latent heat flux associated with snowfall (computed as the product of latent heat of fusion and snowfall rate). Here, we take constant latent heat of vaporization (at 0°C) in the latent heat flux term that is contained in F_s but variations in latent heat flux arising from the deviation of evaporated water from 0°C are contained in F_{PE}, which additionally accounts for sensible heat of precipitation (referenced to 0°C). That is, F_{PE} expresses

445 a modification of F_s arising from global evaporation and precipitation occurring at temperatures
446 different from 0°C.

447 Snowfall is the fraction of precipitation that returns originally evaporated water to the surface in a
448 frozen state. In that sense, F_{snow} represents a heat transfer from the surface to the atmosphere: it
449 warms the atmosphere through additional latent heat release (associated with freezing of vapor)
450 and snowfall consequently arrives at the surface in an energetic state lowered by this latent heat.
451 This energetic effect is most obvious over the open ocean, where falling snow requires the same
452 amount of latent heat to be melted again and thus cools the ocean. Over high latitudes, F_{snow} can
453 attain values up to 5 Wm^{-2}, but its global average value is smaller than 1 Wm^{-2} (Mayer et al., 2017).
454 Although its global mean energetic effect is relatively small, it is systematic and should be included
455 for accurate diagnostics. Moreover, snowfall is an important contributor to the heat and mass
456 budget of ice sheets and sea ice (see section 4).

457 F_{PE} represents the net heat flux arising from the different temperatures of rain and evaporated
458 water. This flux can be sizable regionally, but it is small in a global average sense (warming of the
459 atmosphere ~0.3 Wm^{-2} according to Mayer et al., 2017).

460 Equation 3 provides a decomposition of the atmospheric energy content AE into sensible heat
461 energy (sum of the first two terms, internal heat energy and gravity potential energy), latent heat
462 energy (third term) and kinetic energy (fourth term), where ρ is the air density, c_v the specific heat
463 for moist air at constant volume, T the air temperature, g the acceleration of gravity, L_e the
464 temperature-dependent effective latent heat of condensation (and vaporization) L_v or sublimation
465 L_s (the latter relevant below 0 °C), q the specific humidity of the moist air, and V the wind speed.
466 We neglect atmospheric liquid water droplets and ice particles as separate species, as their amounts
467 and especially their trends are small.

468 In the AE derivation from observational datasets based on Equation 3, we accounted for the
469 intrinsic temperature dependence of the latent heat of water vapor by assigning L_e to L_v if ambient
470 temperatures are above 0 °C and to L_s (adding in the latent heat of fusion L_f) if they are below –10
471 °C, respectively, with a gradual (half-sine weighted) transition over the temperature range
472 between. The reanalysis evaluations similarly approximated L_e by using values of L_v, L_s, and L_f,
473 though in slightly differing forms. The resulting differences in AE anomalies from any of these
474 choices are negligibly small, however, since the latent heat contribution at low temperatures is
475 itself very small.

476 As another small difference, the AE estimations from observations neglected the kinetic energy
477 term in Equation 3 (fourth term), while the reanalysis evaluations accounted for it. This as well
478 leads to negligible AE anomaly differences, however, since the kinetic energy content and trends
479 at global scale are more than three orders of magnitude smaller than for the sensible heat (Peixoto
480 and Oort, 1992). Aligning with the terminology of ocean heat content (OHC) and given the
481 dominance of the heat-related terms in Equation 3, we hence refer to the energy content AE as
482 atmospheric heat content (AHC) hereafter.

483 Turning to the actual datasets used, atmospheric energy accumulation can be quantified using
484 various data types, as summarized in the following. Atmospheric reanalyses combine

485 observational information from various sources (radiosondes, satellites, weather stations, etc.) and
486 a dynamical model in a statistically optimal way. This data type has reached a high level of
487 maturity, thanks to continuous development work since the early 1990s (Hersbach et al., 2018).
488 Especially reanalysed atmospheric state quantities like temperature, winds, and moisture are
489 considered to be of high quality and suitable for climate studies, although temporal discontinuities
490 introduced from the ever-changing observation system remain a matter of concern (Berrisford et
491 al., 2011; Chiodo & Haimberger, 2010).

492 Here we use the current generation of atmospheric reanalyses as represented by ECMWF's fifth-
493 generation reanalysis ERA5 (Hersbach et al., 2018, 2020), NASA's Modern-Era Retrospective
494 analysis for Research and Applications version 2 (MERRA2) (Gelaro et al., 2017), and JMA's 55-
495 year-long reanalysis JRA55 (Kobayashi et al., 2015). All these are available over 1980 to 2018
496 (ERA5 also in 1979) while JRA55 is the only one covering the full early timeframe 1960 to 1979.
497 We additionally used a different version of JRA55 that assimilates only conventional observations
498 also over the satellite era from 1979 onwards, which away from the surface only leaves radiosondes
499 as data source and which is available to 2012 (JRA55C). The advantage of this product is that it
500 avoids potential spurious jumps associated with satellite changes. Moreover, JRA55C is fully
501 independent of satellite-derived Global Positioning System (GPS) radio occultation (RO) data that
502 are also separately used and described below together with the observational techniques.

503 In addition to these four reanalyses, the datasets from three different observation techniques have
504 been used for complementary observational estimates of the atmospheric heat content (AHC). We
505 use the Wegener Center (WEGC) multi-satellite RO data record, WEGC OPSv5.6 (Angerer et al.,
506 2017) as well as its radiosonde (RS) data record derived from the high-quality Vaisala sondes
507 RS80/RS92/VS41, WEGC Vaisala (Ladstädter et al., 2015). WEGC OPSv5.6 and WEGC Vaisala
508 provide thermodynamic upper air profiles of air temperature, specific humidity, and density from
509 which we locally estimate the vertical AHC based on the first three integral terms of Equation 3
510 (Kirchengast et al., 2019). In atmospheric domains not fully covered by the data (e.g., in the lower
511 part of the boundary layer for RO or over the polar latitudes for RS) the profiles are vertically
512 completed by collocated ERA5 information. The local vertical AHC results are then averaged into
513 regional monthly means, which are finally geographically aggregated to global AHC. Applying
514 this estimation approach in the same way to reanalysis profiles sub-sampled at the observation
515 locations accurately leads to the same AHC anomaly time series records as the direct estimation
516 from the full gridded fields.

517 The third observation-based AHC dataset derives from a rather approximate estimation approach
518 using the microwave sounding unit (MSU) data records (Mears & Wentz, 2017). Because the very
519 coarse vertical resolution of the brightness temperature measurements from MSU does not enable
520 integration according to Equation 3, this dataset is derived by replicating the method used in IPCC
521 AR5 WGI Assessment Report 2013 (Rhein, M., et al., 2013; Chap. 3, Box 3.1 therein). We used
522 the most recent MSU Remote Sensing System (RSS) V4.0 temperature dataset (Mears and Wentz,
523 2017), however, instead of MSU RSS V3.3 that was used in the IPCC AR5 (Mears & Wentz,
524 2009a, 2009b) (updated to version 3.3). In order to derive global time series of AHC anomalies,
525 the approach simply combines weighted MSU lower tropospheric temperature and lower
526 stratospheric temperature changes (TLT and TLS channels) converted to sensible heat content

527   changes via global atmospheric mass, and an assumed fractional increase of latent heat content
528   according to water vapor content increase driven by temperature at a near-Clausius-Clapeyron rate
529   (7.5 %/°C).

530   Figure 3 shows the resulting global AHC change inventory over 1980 to 2018 in terms of AHC
531   anomalies of all data types (top), mean anomalies and time-average uncertainty estimates including
532   long-term AHC trend estimates (middle), and annual-mean AHC tendency estimates (bottom). The
533   mean anomaly time series (middle left), preceded by the small JRA55 anomalies over 1960-1979
534   is used as part of the overall heat inventory in Section 5 below. Results including MSU in addition
535   are separately shown (right column), since this dataset derives from a fairly approximate
536   estimation as summarized above and hence is given lower confidence than the others deriving from
537   rigorous AHC integration & aggregation. Since it was the only dataset for AHC change estimation
538   in the IPCC AR5 report, bringing it into context is considered relevant, however.

539   The results clearly show that the AHC trends have intensified from the earlier decades represented
540   by the 1980-2010 trends of near 1.8 TW (consistent with the trend interval used in the IPCC AR5
541   report). We find the trends about 2.5 times higher over 1993-2018 (about 4.5 TW) and about three
542   times higher in the most recent two decades over 2002-2018 (near 5.3 TW), a period that is already
543   fully covered also by the RO and RS records (which estimate around 6 TW). Checking the
544   sensitivity of these long-term trend estimates to ENSO interannual variations, by comparing trend
545   fits to ENSO-corrected AHC anomalies (with ENSO regressed out via the Nino 3.4 Index),
546   confirms that the estimates are robust.

547   The year-to-year annual-mean tendencies in AHC, reaching amplitudes as high as 50 to 100 TW
548   (or 0.1 to 0.2 Wm^{-2}, if normalized to the global surface area), indicate the strong coupling of the
549   atmosphere with the uppermost ocean. This is mainly caused by the ENSO interannual variations
550   that lead to net energy changes in the climate system including the atmosphere (Loeb et al., 2012;
551   Mayer et al., 2013) and substantial reshuffling of heat energy between the atmosphere and the
552   upper ocean (Lijing Cheng, Trenberth, et al., 2019; Johnson & Birnbaum, 2017; Mayer et al., 2014,
553   2016).

554
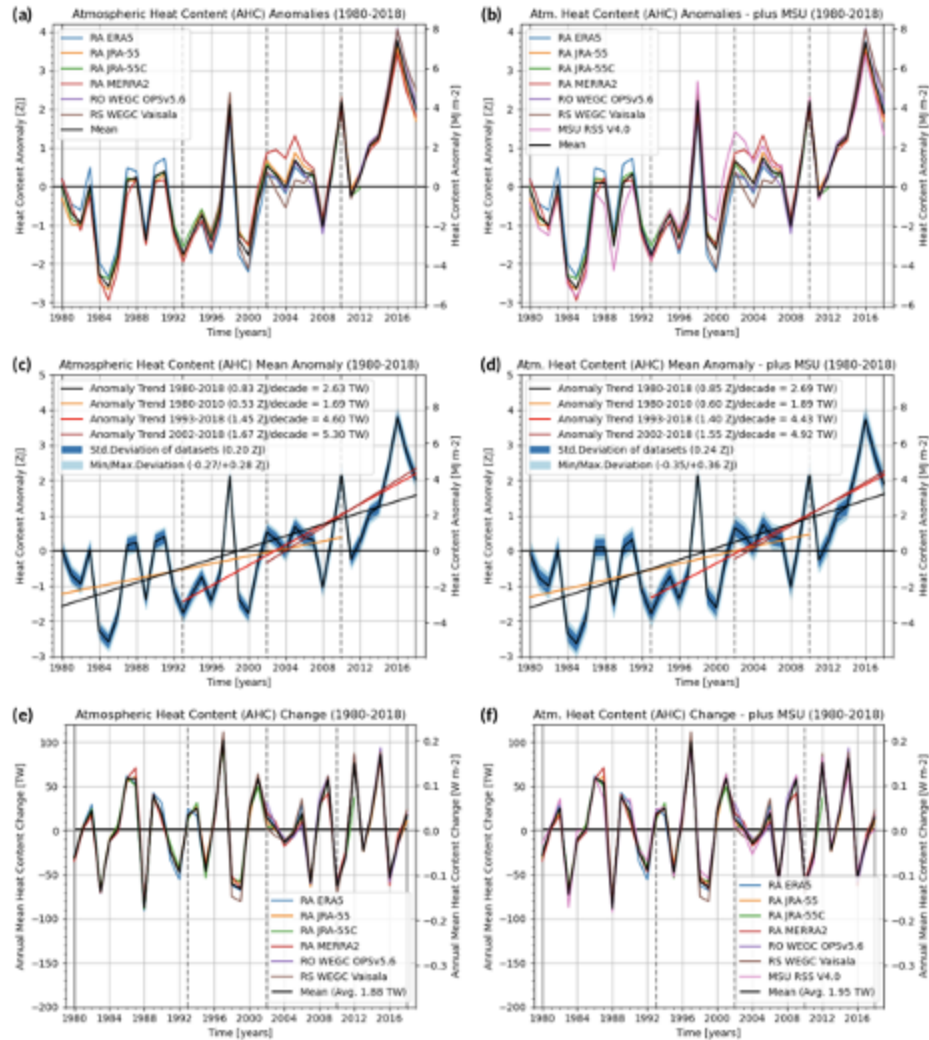
Figure 3: *Annual-mean global AHC anomalies over 1980 to 2018 of four different reanalyses and two (left)*
or three (right, plus MSU) different observational datasets shown together with their mean (top), the mean
AHC anomaly shown together with four representative AHC trends and ensemble spread measures of its
underlying datasets (middle), and the annual-mean AHC change (annual tendency) shown for each year
over 1980 to 2018 for all datasets and their mean (bottom). The in-panel legends identify the individual
datasets shown (top and bottom) and the chosen trend periods together with the associated trend values
and spread measures (middle), the latter including the time-average standard deviation and
minimum/maximum deviations of the individual datasets from the mean.

3. Heat available to warm land

Although the land component of the Earth's energy budget accounts for a small proportion of heat
in comparison with the ocean, several land-based processes sensitive to the magnitude of the
available land heat play a crucial role in the future evolution of climate. Among others, the stability

and extent of the continental areas occupied by permafrost soils depend on the land component. Alterations of the thermal conditions at these locations have the potential to release long-term stored CO_2 and CH_4, and may also destabilize the recalcitrant soil carbon (Bailey et al., 2019; Hicks Pries et al., 2017). Both of these processes are potential "tipping points" (Lenton et al., 2019; Lenton, 2011; Lenton et al., 2008) leading to possible positive feedback on the climate system (Leifeld et al., 2019; MacDougall et al., 2012). Increased land energy is related to decreases in soil moisture that may enhance the occurrence of extreme temperature events (Jeong et al., 2016; S. Seneviratne et al., 2006, 2014; S. I. Seneviratne et al., 2010; Xu et al., 2019). Such extreme events carry negative health effects for the most vulnerable sectors of human and animal populations and ecosystems (Matthews et al., 2017; McPherson et al., 2017; Sherwood & Huber, 2010; Watts et al., 2019). Given the importance of properly determining the fraction of EEI flowing into the land component, recent works have examined the CMIP5 simulations and revealed that Earth System Models (ESMs) have shortcomings in modelling the land heat content of the last half of the 20th century (Francisco José Cuesta-Valero et al., 2016). Numerical experiments have pointed to an insufficient depth of the Land Surface Models (LSMs) (MacDougall et al., 2008, 2010; C. W. Stevens, 2007) and to a zero heat-flow bottom boundary condition (BBC) as the origin of the limitations in these simulations. An LSM of insufficient depth limits the amount of energy that can be stored in the subsurface. The zero heat-flow BBC neglects the small but persistent long-term contribution from the flow of heat from the interior of the Earth, that shifts the thermal regime of the subsurface towards or away from the freezing point of water, such that the latent heat component is misrepresented in the northern latitudes (Hermoso de Mendoza et al., 2018). Although the heat from the interior of the Earth is constant at time scales of a few millennia, it may conflict with the setting of the LSM initial conditions in ESM simulations. Modelling experiments have also allowed to estimate the heat content in land water reservoirs (Vanderkelen et al., 2020), accounting for 0.3±0.3 ZJ from 1900 to 2020. Nevertheless, this estimate has not been included here because it is derived from model simulations and its magnitude is small in relation to the rest of components of the Earth's heat inventory.

Borehole Climatology

The main premise of borehole climatology is that the subsurface thermal regime is determined by the balance of the heat flowing from the interior of the Earth (the bottom boundary condition) and the heat flowing through the interface between the lower atmosphere and the ground (the upper boundary condition). If the thermal properties of the subsurface are known, or if they can be assumed constant over short-depth intervals, then the thermal regime of the subsurface can be determined by the physics of heat diffusion. The simplest analogy is the temperature distribution along a (infinitely wide) cylinder with known thermal properties and constant temperature at both ends. If upper and lower boundary conditions remain constant (i.e. internal heat flow is constant, and there are no persistent variations on the ground surface energy balance), then the thermal

regime of the subsurface is well known and it is in a (quasi) steady state. However, any change to the ground surface energy balance would create a transient, and such a change in the upper boundary condition would propagate into the ground leading to changes in the thermal regime of the subsurface (Beltrami, 2002a). These changes in the ground surface energy balance propagate into the subsurface and are recorded as departures from the quasi-steady thermal state of the subsurface. Borehole climatology uses these subsurface temperature anomalies to reconstruct the ground surface temperature changes that may have been responsible for creating the subsurface temperature anomalies we observe. That is, it is an attempt to reconstruct the temporal evolution of the upper boundary condition. Ground Surface Temperature Histories (GSTHs) and Ground Heat Flux Histories (GHFHs) have been reconstructed from borehole temperature profile (BTP) measurements at regional and larger scales for decadal and millennial time-scales (Barkaoui et al., 2013; Beck, 1977; Beltrami, 2001; Beltrami et al., 2006; Beltrami & Bourlon, 2004; Cermak, 1971; Christian Chouinard & Mareschal, 2009; Davis et al., 2010; Demezhko & Gornostaeva, 2015; Harris & Chapman, 2001; Hartmann & Rath, 2005; Hopcroft et al., 2007; Huang et al., 2000; Jaume-Santero et al., 2016; Lachenbruch & Marshall, 1986; Lane, 1923; Pickler et al., 2018; Roy et al., 2002; Vasseur et al., 1983). These reconstructions have provided independent records for the evaluation of the evolution of the climate system well before the existence of meteorological records. Because subsurface temperatures are a direct measure, which unlike proxy reconstructions of past climate do not need to be calibrated with the meteorological records, they provide an independent way of assessing changes in climate. Such records, are useful tools for evaluating climate simulations prior to the observational period (Beltrami et al., 2017; Cuesta-Valero et al., 2019; Cuesta-Valero et al., 2016; García-García et al., 2016; González-Rouco et al., 2006; Jaume-Santero et al., 2016; MacDougall et al., 2010; Stevens et al., 2008), as well as for assessing proxy data reconstructions (Beltrami et al., 2017; Jaume-Santero et al., 2016).

Borehole reconstructions have, however, certain limitations. Due to the nature of heat diffusion, temperature changes propagated through the subsurface suffer both a phase shift and an amplitude attenuation (Smerdon & Stieglitz, 2006). Although subsurface temperatures continuously record all changes in the ground surface energy balance, heat diffusion filters out the high frequency variations of the surface signal with depth, thus the annual cycle is detectable up to approximately 16 m of depth, while millennial changes are recorded approximately to a depth of 500 m. Therefore, reconstructions from borehole temperature profiles represent changes at decadal to millennial time scales. Additionally, borehole data are sparse, since the logs were usually recorded from holes of opportunity at mining exploration sites. As a result, the majority of profiles were measured in the Northern Hemisphere, although recent efforts have been taken to increase the sampling rate in South America (Pickler et al., 2018) and Australia (Suman et al., 2017). Despite this uneven sampling, the spatial distribution of borehole profiles has been able to represent the evolution of land surface conditions at global scales (Beltrami & Bourlon, 2004; Cuesta-Valero et al., 2020; González-Rouco et al., 2006, 2009; Pollack & Smerdon, 2004). Another factor that reduces the number of borehole profiles suitable for climate analyses is the presence of non-

648 climatic signals in the measured profiles, mainly caused by groundwater flow and changes in the
649 lithology of the subsurface. Therefore, all profiles are screened before the analysis in order to
650 remove questionable logs. Despite all these limitations, the borehole methodology has been shown
651 to be reliable based on observational analyses (Bense & Kooi, 2004; C Chouinard & Mareschal,
652 2007; Pollack & Smerdon, 2004; Verdoya et al., 2007) and pseudo-proxy experiments
653 (García Molinos et al., 2016; González-Rouco et al., 2006, 2009).

654

655 **Land Heat Content Estimates**

656

657 Global continental energy content has been previously estimated from geothermal data retrieved
658 from a set of quality-controlled borehole temperature profiles. Ground heat content was estimated
659 from heat flux histories derived from BTP data (Beltrami, 2002b; Beltrami et al., 2002, 2006).
660 Such results have formed part of the estimate used in AR3, AR4 and AR5 IPCC reports (see Box
661 3.1, Chapter 3 (Rhein et al., 2013). A continental heat content estimate was inferred from
662 meteorological observations of surface air temperature since the beginning of the 20th century
663 (Huang, 2006). Nevertheless, all global estimates were performed nearly two decades ago. Since,
664 those days, advances in borehole methodological techniques (Beltrami et al., 2015; Cuesta-Valero
665 et al., 2016; Jaume-Santero et al., 2016), the availability of additional BTP measurements, and the
666 possibility of assessing the continental heat fluxes in the context of the FluxNet measurements
667 (Gentine et al., 2020) requires a comprehensive summary of all global ground heat fluxes and
668 continental heat content estimates.

669

Reference	Time period	Heat Flux (mWm^{-2})	Heat Content (ZJ)	Source of Data
(Beltrami, 2002b)	1950-2000	33	7.1	Geothermal
Beltrami et al. (2002)	1950-2000	39.1 (3.5)	9.1 (0.8)	Geothermal
Beltrami et al. (2002)	1900-2000	34.1 (3.4)	15.9 (1.6)	Geothermal
(Beltrami, 2002b)	1765-2000	20.0 (2.0)	25.7 (2.6)	Geothermal
Huang (2006)	1950-2000	-	6.7	Meteorological
Gentine et al (2020)	2004-2015	240 (120)	-	FluxNet, Geothermal, LSM
Cuesta-Valero et al (2020)	1950-2000	70 (20)	16 (3)	Geothermal
Cuesta-Valero et al (2020)	1993-2018	129 (28)	14 (3)	Geothermal
Cuesta-Valero et al., (2020)	2004-2015	136 (28)	6 (1)	Geothermal

670 *Table 2. Ground surface heat flux and global continental heat content. Uncertainties in parenthesis.*

671

672
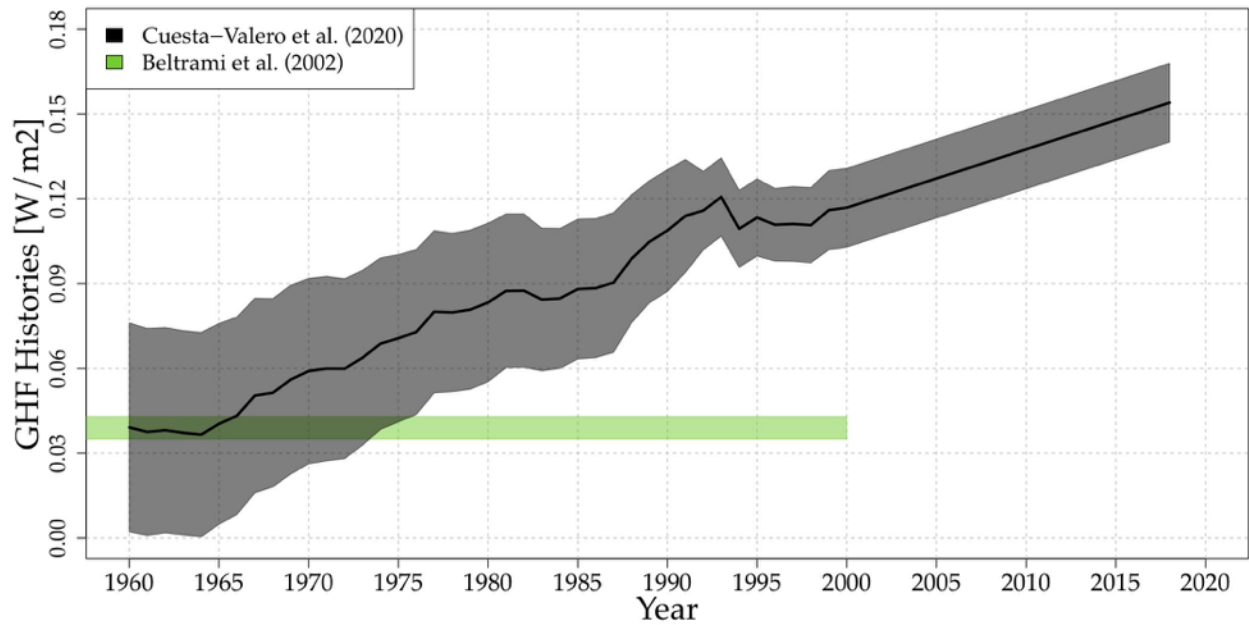
675 **Figure 4:** *Global mean ground heat flux history (black line) and 95% confidence interval (gray shadow)*
676 *from BTP measurements from Cuesta-Valero et al. (2020). Results for 1950-2000 from Beltrami et al.*
677 *(2002) (green bar) are provided for comparison purposes.*

678
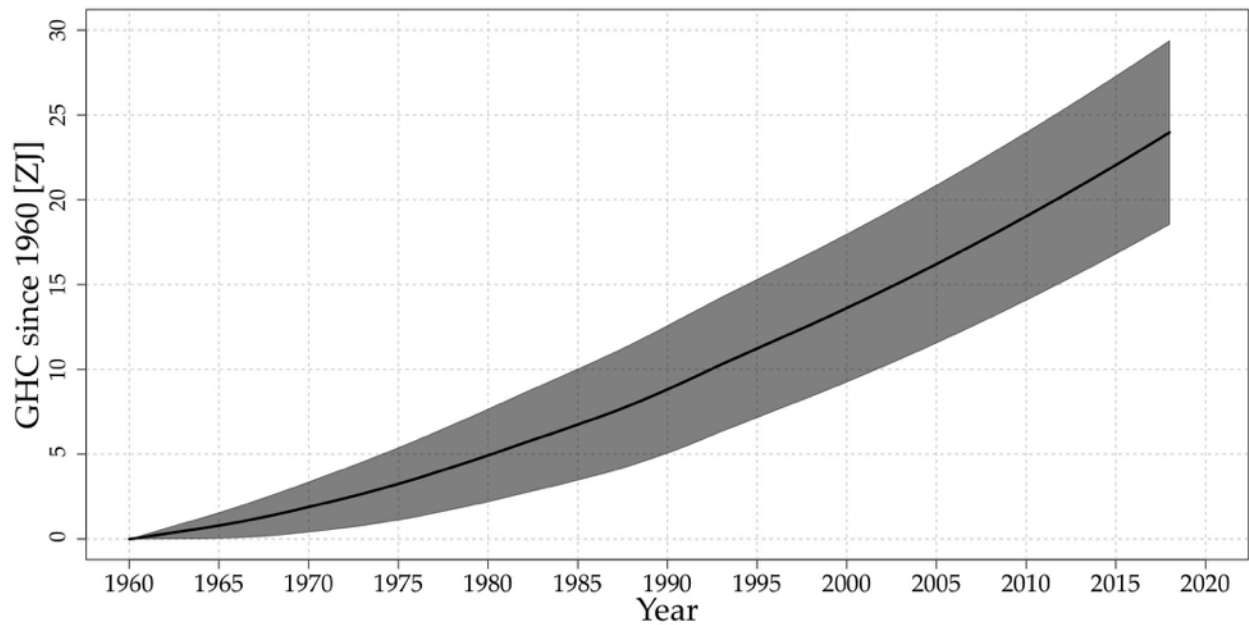
679

680 **Figure 5:** *Global cumulative heat storage within continental landmasses since 1960 CE (black line) and*
681 *95% confidence interval (gray shadow) estimated from GHF results displayed in Fig.4. Data obtained from*
682 *Cuesta-Valero et al. (2020).*

The first estimates of continental heat content used borehole temperature versus depth profile data. However, the dataset in those analyses included borehole temperature profiles of a wide range of depths, as well as different data acquisition dates. That is, each borehole profile contained the record of the accumulation of heat in the subsurface for different time intervals. In addition, the borehole data were analyzed for a single ground surface temperature model using a single constant value for each of the subsurface thermal properties.

Although the thermal signals are attenuated with depth, which may partially compensate for data shortcomings, uncertainties were introduced in previous analyses that may have affected the estimates of subsurface heat change. A continental heat content change estimate was carried out using a gridded meteorological product of surface air temperature by (Huang, 2006). Such work yielded similar values as the estimates from geothermal data (see Table 2). This estimate, however, assumed that surface air and ground temperatures are perfectly coupled everywhere, and used a single value for the thermal conductivity of the ground. Studies have shown that the coupling of the surface air and ground temperatures is mediated by several processes that may influence the ground surface energy balance, and therefore, the air-ground temperature coupling (García-García et al., 2019; Melo-Aguilar et al., 2018; Stieglitz & Smerdon, 2007). In a novel attempt to reconcile continental heat content from soil heat-plate data from the FluxNet network with estimates from geothermal data and a deep bottom-boundary land surface model simulation, (Gentine et al., 2020) obtained a much larger magnitude from the global land heat flux than all previous estimates. Cuesta-Valero et al. (2020) has recently updated the estimate of the global continental heat content using a larger borehole temperature database (1079 logs) that includes more recent measurements and a stricter data quality control. The updated estimate of continental heat content change also takes into account the differences in borehole logging time and restricts the data to the same depth range for each borehole temperature profile. Such depth range restriction ensures that the subsurface accumulation of heat at all BTP sites is synchronous. In addition to the standard method for reconstructing heat fluxes with a single constant value for each subsurface thermal property, Cuesta-Valero et al. (2020) also developed a new approach that considers a range of possible subsurface thermal properties, several models, each at a range of resolutions yielding a more realistic range of uncertainties for the fraction of the EEI flowing into the land subsurface.

Global land heat content estimates from FluxNet data, geothermal data and model simulations point to a marked increase in the amount of energy flowing into the ground in the last few decades (Fig. 4, 5 and Table 2). These results are consistent with the observations of ocean, cryosphere and atmospheric heat storage increases during the same time period and with EEI at the top of the atmosphere.

4. Heat utilized to melt ice

The energy uptake by the cryosphere is given by the sum of the energy uptake within each one of its components: sea-ice, the Greenland and Antarctic ice sheets, glaciers other than those that are part of the ice sheets ('glaciers', hereafter), snow and permafrost. The basis for the heat uptake by

723 the cryosphere presented here is provided by a recent estimate for the period 1979 to 2017 (F.
724 Straneo et al., 2020). This study concludes that heat uptake over this period is dominated by the
725 mass loss from Arctic sea-ice, glaciers and the Greenland and Antarctic ice sheets. The
726 contributions from thawing permafrost and shrinking snow cover are either negligible, compared
727 to these other components, or highly uncertain. (Note that warming of the land in regions where
728 permafrost is present is accounted for in the land-warming, however, the energy to thaw the
729 permafrost is not). Antarctic sea-ice shows no explicit trend over the period described here
730 (Parkinson, 2019). Here, we extend the estimate of Straneo et al. 2020 backwards in time to 1960
731 and summarize the method, the data and model outputs used. The reader is referred to Straneo et
732 al. (2020) for further details.
733
734 Within each component of the cryosphere, energy uptake is dominated by that associated with
735 melting; including both the latent heat uptake and the warming of the ice to its freezing point. As
736 a result, the energy uptake by each component is directly proportional to its mass loss (Straneo et
737 al., 2020). For consistency with previous estimates (Ciais et al., 2013), we use a constant latent
738 heat of fusion of 3.34×10^5 J/kg, a specific heat capacity of 2.01×10^3 J/kg C and an ice density of
739 920 kg/m^3.
740
741 For Antarctica, we separate contributions from grounded ice loss and floating ice loss building on
742 recent separate estimates for each. Grounded ice loss from 1992 to 2017 is based on a recent study
743 that reconciles mass balance estimates from gravimetry, altimetry and input-output methods from
744 1992 to 2017 (Shepherd, Ivins, et al., 2018). For the 1972-1991 period, we used estimates from
745 (Rignot et al., 2019), which combined modeled surface mass balance with ice discharge estimates
746 from the input/output method. Floating ice loss between 1994 and 2017 is based on thinning rates
747 and iceberg calving fluxes estimated using new satellite altimetry reconstructions (Adusumilli et
748 al., 2019). For the 1960–1994 period, we also considered mass loss from declines in Antarctic
749 Peninsula ice shelf extent (Cook & Vaughan, 2010) using the methodology described in Straneo
750 et al. (2020).
751
752 To estimate grounded ice mass loss in Greenland, we use the Ice Sheet Mass Balance
753 Intercomparison Exercise for the time period 1992-2017 (Shepherd et al., 2020) and the difference
754 between surface mass balance and ice discharge for the period 1979-1991 (Mankoff et al., 2019;
755 Mouginot et al., 2019; Noël et al., 2018). Due to a lack of observations, from 1960-1978 we
756 assume no mass loss. For floating ice mass change, we collated reports of ice shelf thinning and/or
757 collapse together with observed tidewater glacier retreat (Straneo et al., 2020). Based on firn
758 modeling we assessed that warming of Greenland's firn has not yet contributed significantly to its
759 energy uptake (Ligtenberg et al., 2018; F. Straneo et al., 2020).
760
761 For glaciers we combine estimates for glaciers from the Randolph Glacier Inventory outside of
762 Greenland and Antarctica, based on direct and geodetic measurements (Zemp et al., 2019), with

estimates based on a glacier model forced with an ensemble of reanalysis data (Marzeion et al., 2015) and GRACE based estimates (Bamber et al., 2018). An additional contribution from uncharted glaciers or glaciers that have already disappeared is obtained from (Parkes & Marzeion, 2018). Greenland and Antarctic peripheral glaciers are derived from Zemp et al., (2019) and Marzeion et al. (2015).

Finally, while estimates of Arctic sea-ice extent exist over the satellite record, sea-ice thickness distribution measurements are scarce making it challenging to estimate volume changes. Instead we use the Pan-Arctic Ice Ocean Modeling and Assimilation System (PIOMAS) (Schweiger et al., 2011; Zhang & Rothrock, 2003) which assimilates ice concentration and sea surface temperature data and is validated with most available thickness data (from submarines, oceanographic moorings, and remote sensing; and against multi-decadal records constructed from satellite, e.g. (Labe et al., 2018; Laxon et al., 2013; X. Wang et al., 2016). A longer reconstruction using a slightly different model version, PIOMAS-20C (Schweiger et al., 2019), is used to cover the 1960 to 1978 period that is not covered by PIOMAS.

These reconstructions reveal that all four components contributed similar amounts (between 2-5 ZJ) over the 1960-2017 period amounting to a total energy uptake by the cryosphere of 14.7 +/- 1.9 ZJ. Compared to earlier estimates, and in particular the 8.83 ZJ estimate from (Ciais et al., 2013), this larger estimate is a result both of the longer period of time considered and, also, the improved estimates of ice loss across all components, especially the ice shelves in Antarctica. Approximately half of the Cryosphere's energy uptake is associated with the melting of grounded ice, while the remaining half is associated with the melting of floating ice (ice shelves in Antarctica and Greenland, Arctic sea-ice).

5. The Earth heat inventory: Where does the energy go?

The Earth has been in radiative imbalance, with less energy exiting the top of the atmosphere than entering, since at least about 1970 and the Earth has gained substantial energy over the past 4 decades (Hansen, 2005; Rhein et al., 2013). Due to the characteristics of the Earth system components, the ocean with its large mass and high heat capacity dominates the Earth heat inventory (Cheng et al., 2016, 2017; Rhein et al., 2013; von Schuckmann et al., 2016). The rest goes into grounded and floating ice melt, and warming the land and atmosphere.
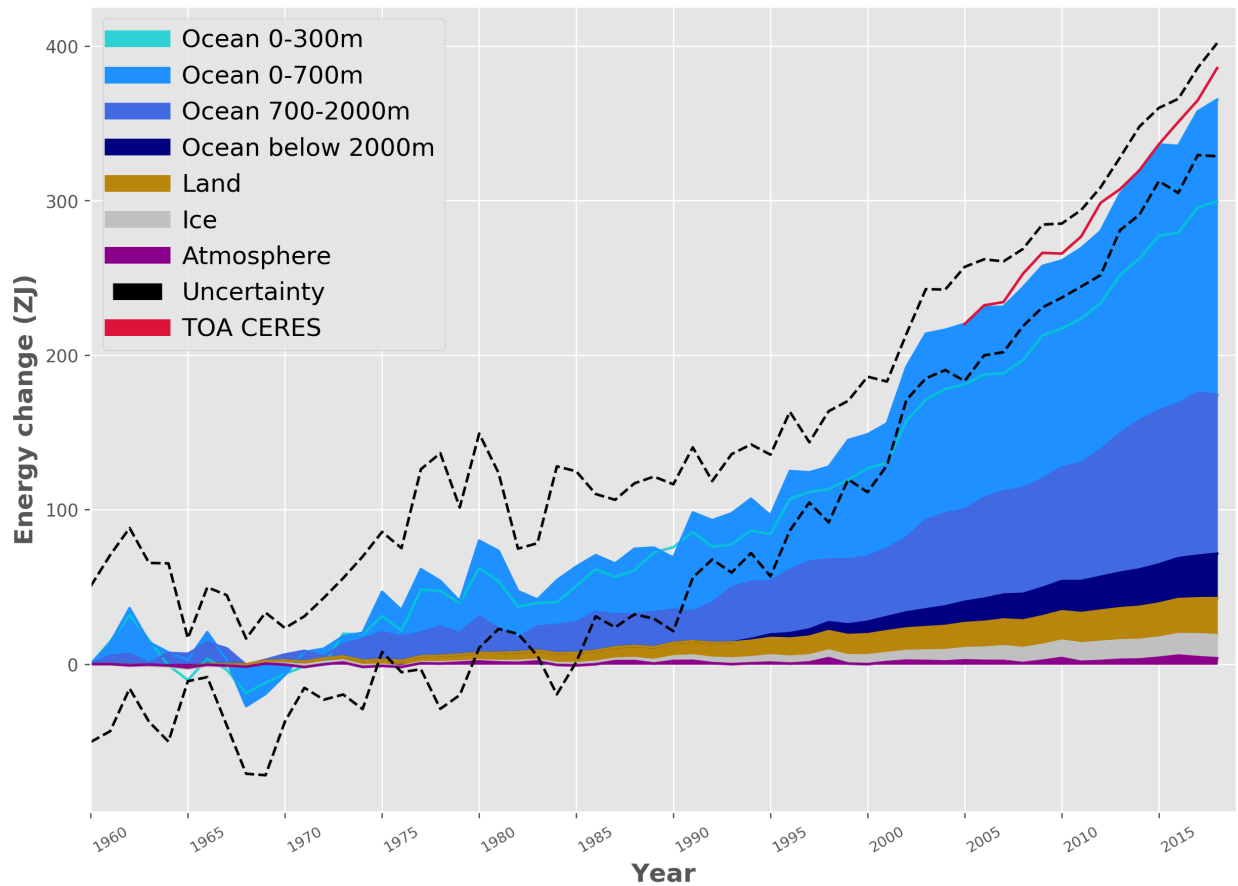
Figure 6: Earth heat inventory (energy accumulation) in ZJ (1 ZJ = 10^{21} J) for the components of the Earth's climate system relative to 1960 and from 1960 to 2018 (assuming constant cryosphere increase for the year 2018). See section 1-4 for data sources. The upper ocean (0-300m, light blue line, and 0-700m, light blue shading) account for the largest amount of heat gain, together with the intermediate ocean (700-2000m, blue shading), and the deep ocean below 2000m depth (dark blue shading). Although much lower, the second largest contributor is the storage of heat on land (orange shading), followed by the gain of heat to melt grounded and floating ice in the cryosphere (gray shading). Due to its low heat capacity, the atmosphere (magenta shading) makes a smaller contribution. Uncertainty in the ocean estimate also dominates the total uncertainty (dot-dashed lines derived from the standard deviations (2-sigma) for the ocean, cryosphere and land. Atmospheric uncertainty is comparably small). Deep ocean (> 2000m) are assumed zero before 1990 (see section 1 for more details). The dataset for the Earth heat inventory is published at DKRZ (https://www.dkrz.de/) under the doi: https://doi.org/10.26050/WDCC/GCOS_EHI_EXP_v2. The net flux at TOA from the NASA CERES program is shown in red (https://ceres.larc.nasa.gov/data/, see also for example Loeb et al., 2012) for the period 2005-2018 to account for the 'golden period' of best available estimates. We obtain a total heat gain of 358 ± 37 ZJ over the period 1971-2018, which is equivalent to a heating rate (i.e. the EEI) of 0.47 ± 0.1 Wm^{-2} applied continuously over the surface area of the Earth (5.10 × 10^{14} m^2). The corresponding EEI over the period 2010-2018 amounts to 0.87 ± 0.12 Wm^{-2}. A weighted least square fit has been used taking into account the uncertainty range (see also von Schuckmann and Le Traon, 2011).

821

822 In agreement with previous studies, the Earth heat inventory based on most recent estimates of
823 heat gain in the ocean (section 1), the atmosphere (section 2), land (section 3) and the cryosphere
824 (section 4) shows a consistent long-term heat gain since the 1960s (Fig. 6). Our results show a total
825 heat gain of 358 ± 37 ZJ over the period 1971-2018, which is equivalent to a heating rate of 0.47
826 ± 0.1 Wm^{-2}, and applied continuously over the surface area of the Earth (5.10×10^{14} m^2). For
827 comparison, the heat gain obtained in IPCC AR5 amounts to 274 ± 78 ZJ and 0.4 Wm^{-2} over the
828 period 1971-2010 (Rhein et al., 2013). In other words, our results show that since the IPCC AR5
829 estimate has been performed, heat accumulation has continued at a comparable rate. The major
830 player in the Earth inventory is the ocean, particularly the upper (0-700m) and intermediate (700-
831 2000m) ocean layers (see also section 1, Fig. 2).

832

833 Although the net flux at TOA as derived from remote sensing are anchored by an estimate of global
834 OHC (Loeb et al., 2012), and thus does not provide a completely independent result for the total
835 EEI, we additionally compare net flux at TOA with the Earth heat inventory obtained in this study
836 (Fig. 6). Both rate of changes compare well, and we obtain 0.7 ± 0.1 Wm^{-2} for the remote sensing
837 estimate at TOA, and 0.8 ± 0.1 Wm^{-2} for the Earth heat inventory over the period 2005-2018.

838

839
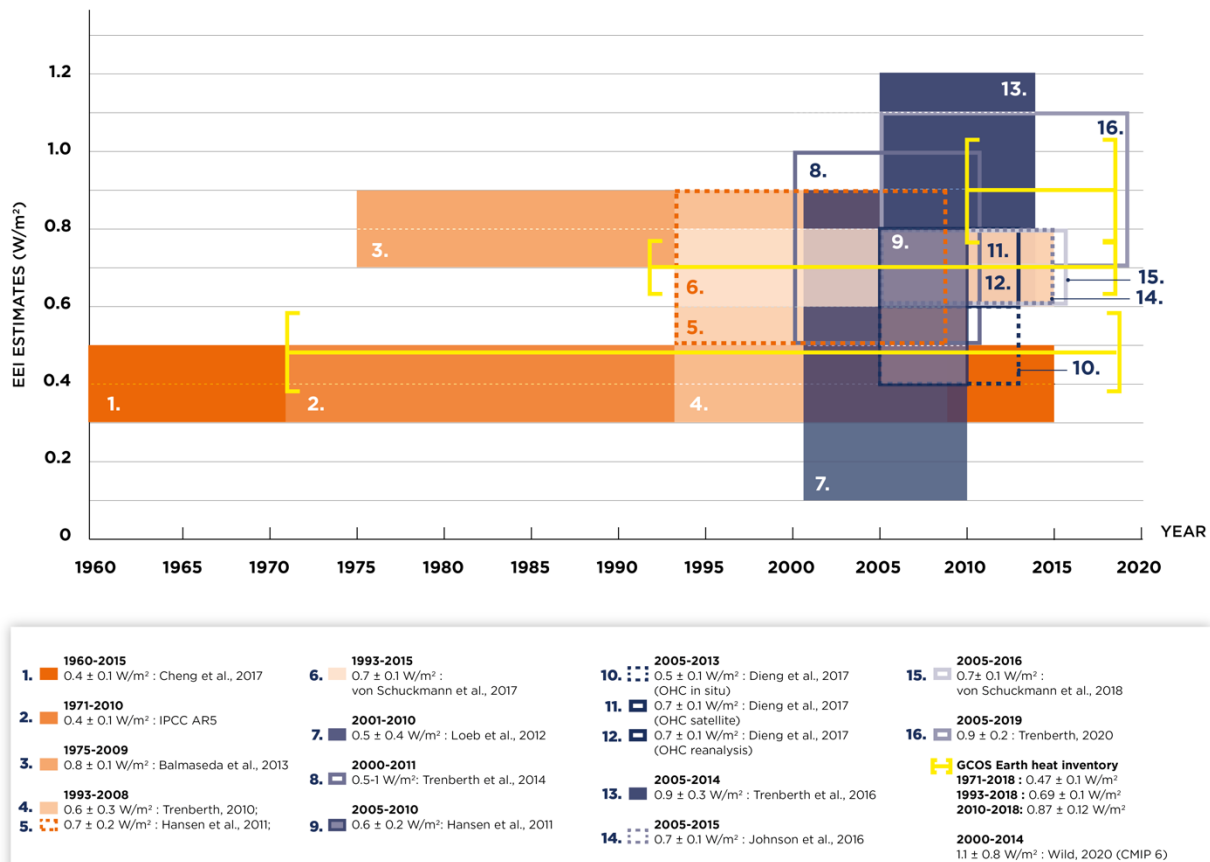
840 **_Fig. 7:_** _Overview on EEI estimates as obtained from previous publications, and references are listed in the_
841 _figure legend. For IPCC AR5, Rhein et al. (2013) is used. The color bars take into account the uncertainty_
842 _ranges provided in each publication, respectively. For comparison, the estimates of our Earth heat_
843 _inventory based on the results of Fig. 6 have been added (yellow lines) for the periods 1971-2018, 1993-_
844 _2018 and 2010-2018, and the trends have been evaluated using a weighted least square fit (see von_
845 _Schuckmann and Le Traon, 2011 for details on the method)._
846
847

848 Rates of change derived from Fig. 6 are in agreement with previously published results for the
849 different periods (Fig. 7). Major disagreements occur for the estimate of Balmaseda et al. (2013)
850 which is obtained from an ocean reanalysis, and known to provide higher heat gain compared to
851 results derived strictly from observations (Meyssignac et al., 2019). Over the last quarter of a
852 decade this Earth heat inventory reports - in agreement with previous publications - an increased
853 rate of Earth heat uptake reaching up to 0.9 W/m^2 (Fig. 7). This period is also characterized with
854 an increase in the availability and quality of the global climate observing system, particularly for
855 the past 2 decades. The heat inventory as obtained in this study reveals an EEI of 0.87 ± 0.12 W/m^2
856 over the period 2010-2018 - a period which experienced record levels of Earth surface warming,
857 and is ranked as the warmest decade relative to the reference period 1850-1900 (WMO, 2020).
858 Whether this increased rate can be attributed to an acceleration of global warming and Earth system
859 heat uptake (e.g. Cheng et al., 2018; WMO, 2020; Blunden and Arndt, 2019), or an induced
860 estimation bias due to the interplay between natural and anthropogenic driven variability (e.g.
861 Cazenave et al., 2014), or underestimated uncertainties in the historical record (e.g. Boyer et al.,
862 2016) needs further investigation.

863

864 The new multidisciplinary estimate obtained from a concerted international effort provides an
865 updated insight in where the heat is going from a positive EEI of 0.47 ± 0.1 W/m^2 for the period
866 1971-2018. Over the period 1971-2018 (2010-2018), 89% (90%) of the EEI is stored in the global
867 ocean, from which 52% (52%) is repartitioned in the upper 700m depth and 28% (30%) at
868 intermediate layers (700-2000m), and 9% (8%) in the deep ocean layer below 2000m depth.
869 Atmospheric warming amounts to 1% (2%) in the Earth heat inventory, the land heat gain with
870 6% (5%) and the heat uptake by the cryosphere with 4% (3%). These results show general
871 agreement with previous estimates (e.g. Rhein et al., 2013). Over the period 2010-2018, the EEI
872 amounts to 0.87 ± 0.12 W/m^2, indicating a rapid increase in EEI over the past decade. Note that a
873 near-global (60°N-60°S) area for the ocean heat uptake is used in this study, which could induce
874 a slight underestimation, and needs further evaluation in the future (see section 1). However, a test
875 using a single dataset (Cheng et al., 2017) indicates that the ocean contribution within 1960-2018
876 can increase by 1% if the full global ocean domain is used (not shown).
877
878
879
880

6. Conclusion

The UN 2030 Agenda for Sustainable Development states that climate change is "one of the greatest challenges of our time…" and warns "…the survival of many societies, and of the biological support systems of the planet, is at risk" (UNGA, 2015). The outcome document of the Rio+20 Conference, *The Future We Want*, defines climate change as "an inevitable and urgent global challenge with long-term implications for the sustainable development of all countries" (UNGA, 2012). The Paris agreement builds upon the United Nations Framework Convention on Climate Change (UN, 1992) and for the first time all nations agreed to undertake ambitious efforts to combat climate change, with the central aim to keep global temperature rise this century well below 2°C above pre-industrial levels and to limit the temperature increase even further to 1.5°C (UN, 2015). Article 14 of the Paris Agreement requires the *Conference of the Parties serving as the meeting of the Parties to the Paris Agreement* (CMA) to periodically take stock of the implementation of the Paris Agreement and to assess collective progress towards achieving the purpose of the Agreement and its long-term goals through the so called global stocktake based on best available science.

The EEI is the most critical number defining the prospects for continued global warming and climate change (Hansen et al., 2011, von Schuckmann et al., 2016), and we call for an implementation of the EEI into the global stocktake. The current positive EEI is understood to be foremost and primarily a result of increasing atmospheric greenhouse gases (IPCC, 2013), which have - according to the IPCC special report on Global Warming of 1.5 ºC - already 'caused approximately 1.0°C of global warming above pre-industrial levels, with a likely range of 0.8°C to 1.2°C' (IPCC, 2018). The IPCC special report further states with high confidence that 'global warming is likely to reach 1.5°C between 2030 and 2052 if it continues to increase at the current rate'. The EEI is the portion of the forcing that the Earth's climate system has not yet responded to (Hansen et al., 2005), and defines additional global warming that will occur without further change in forcing (Hansen et al., 2017). Our results show that EEI is not only continuing, it is increasing. Over the period 1971-2018 average EEI amounts to 0.47 ± 0.12 W/m^2, but amounts to 0.87 ± 0.12 W/m^2 during 2010-2018 (Fig. 8). Concurrently, acceleration of sea level rise (WCRP, 2018; Legelais et al., 2020), accelerated surface warming and record temperatures in the Arctic (Richter-Menge et al., 2019; WMO, 2020) and ice loss from the Greenland ice sheet (King et al., 2020), and intensification of atmospheric warming near-surface and in the troposphere (Steiner et al., 2020) have been - for example - recently reported. To what degree these changes are intrinsically linked needs further evaluations.

EARTH ENERGY IMBALANCE :
⚙ < ☀ 0.47 ± 0.1 (0.87 ± 0.12) W/m²
⚙ ≈ ☀ Required CO₂ reduction : - 57 ppm

INCOMING SOLAR RADIATION

OUTGOING RADIATION

ATMOSPHERE
1% (2%)

TOTAL HEAT GAIN
358 ± 37 ZJ

CRYOSPHERE
4% (3%)

LAND
6% (5%)

OCEAN
89% (90%)
0 - 700 m: **52%** (52%);
700-2000m: **28%** (30%);
> 2000m: **9%** (8%);

1971-2018 (2010-2018)
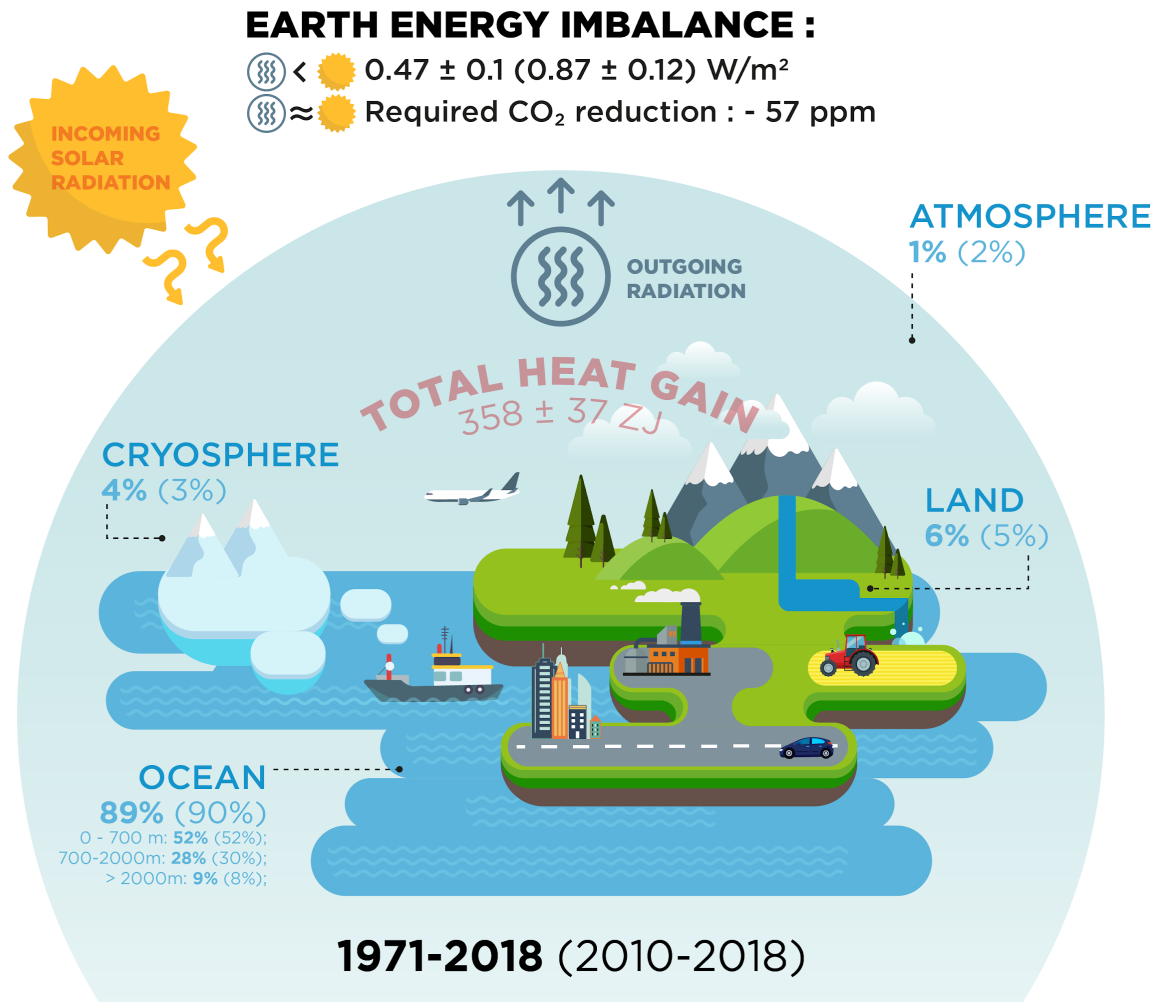
918
919 ***Figure 8:*** *Schematic presentation on the Earth heat inventory for the current anthropogenic driven positive*
920 *Earth energy imbalance at the Top Of the Atmosphere (TOA). Relative partition (in %) of the Earth heat*
921 *inventory presented in Fig. 6 for the different components are given for the ocean (upper: 0-700m,*
922 *intermediate: 700-2000m, deep: > 2000m), land, cryosphere (grounded and floating ice) and atmosphere,*
923 *for the periods 1971-2018 and 2010-2018 (for the latter period values are provided in parentheses), as well*
924 *as for the EEI. The total heat gain (in red) over the period 1971-2018 is obtained from the Earth heat*
925 *inventory as presented in Fig. 6. To reduce the 2010-2018 EEI of 0.87 ± 0.12 W/m² to zero, current*
926 *atmospheric CO_2 would need to be reduced by -57 ± 8 ppm (see text for more details).*

927

928   Global atmospheric CO2 concentration reached 407.38 ± 0.1 ppm averaged over 2018
929   (Friedlingstein et al., 2019). WMO (2020) reports CO_2 concentrations at the Mauna Loa
930   measurement platform of 411.75 ppm in February 2019, and 414.11 ppm in February 2020.
931   Stabilization of climate, the goal of the universally agreed UNFCCC (UN, 1992) and the Paris
932   Agreement (UN, 2015), requires that EEI be reduced to approximately zero to achieve Earth's
933   system quasi-equilibrium. The change of heat radiation to space for a given greenhouse gas change
934   can be computed accurately. The amount of CO_2 in the atmosphere would need to be reduced from

935 410 ppm to 353 ppm (i.e. a required reduction of -57 ± 8 ppm) to increase heat radiation to space
936 by 0.87 W/m^2, bringing Earth back towards energy balance (Fig. 8), where we have used the
937 analytic formulae of Hansen et al. (2000) for this estimation. Atmospheric CO_2 was last 350 ppm
938 in the year 1988, and global Earth's surface temperature was then +0.5°C relative to the pre-
939 industrial period (relative to the 1880-1920 mean) (Hansen et al., 2017; Friedlingstein et al., 2019).
940 In principle, we could reduce other greenhouse gases, and thus require a less stringent reduction
941 of CO_2. However, as discussed by Hansen et al. (2017), some continuing increase of N_2O, whose
942 emissions are associated with food production, seems inevitable, so there is little prospect for much
943 net reduction of non-CO_2 greenhouse gases, and thus, the main burden for climate stabilization
944 falls on CO_2 reduction. This simple number, EEI, is the most fundamental metric that the scientific
945 community and public must be aware of, as the measure of how well the world is doing in the task
946 of bringing climate change under control (Fig. 8).

947

948 This community effort also addresses gaps for the evolution of future observing systems for a
949 robust and continued assessment of the Earth heat inventory, and its different components.
950 Immediate priorities include the maintenance and extension of the global climate observing system
951 to assure a continuous monitoring of the Earth heat inventory, and to reduce the uncertainties. For
952 the global ocean observing system, the core Argo sampling needs to be sustained, and
953 complemented by remote sensing data. Extensions such as into the deep ocean layer need to be
954 further fostered (Desbruyères et al., 2017; Johnson et al., 2015), and technical developments for
955 the measurements under ice and in shallower areas need to be sustained and extended. Moreover,
956 continued efforts are needed to further advance bias correction methodologies, uncertainty
957 evaluations and data processing of the historical dataset.

958

959 In order to allow for improvements on the present estimates of changes in the continental heat and
960 to ensure that the database is continued into the future, an international, coordinated effort is
961 needed to increase the number of subsurface temperature data from BTPs at additional locations
962 around the world, in particular in the southern hemisphere. Additionally, repeated monitoring
963 (after a few decades) of existing boreholes should help reduce uncertainties at individual sites.
964 Such data should be shared through an open platform.

965

966 For the atmosphere, the continuation of operational satellite- and ground-based observations is
967 important but the foremost need is sustaining and enhancing a coherent long-term monitoring
968 system for the provision of climate data records of essential climate variables. GNSS radio
969 occultation observations and reference radiosonde stations within the Global Climate Observing
970 System (GCOS) Reference Upper Air Network (GRUAN) are regarded as climate benchmark
971 observations. Operational radio occultation missions for continuous global climate observations
972 need to be maintained and expanded, ensuring global coverage over all local times, as the central
973 node of a global climate observing system.

974

975 For the cryosphere, sustained remote sensing for all of the cryosphere components is key to
976 quantifying future changes over these vast and inaccessible regions, but must be complemented by
977 in-situ observations for calibration and validation. For sea-ice, the albedo, the area and ice
978 thickness are all essential, with ice-thickness being particularly challenging to quantify with
979 remote sensing alone. For ice sheets and glaciers, reliable gravimetric measurements, ice thickness
980 and extent, snow/firn thickness and density are essential to quantify changes in mass balance of
981 grounded and floating ice. We highlight Antarctic sea-ice change and warming of firn as terms
982 that are poorly constrained or have not significantly contributed to this assessment but may become
983 important over the coming decades. Similarly, there exists the possibility for rapid change
984 associated with positive ice dynamical feedbacks at the marine margins of the Greenland and
985 Antarctic ice sheets. Sustained monitoring of each of these components will, therefore, serve the
986 dual purpose of furthering understanding of the dynamics and quantifying the contribution to
987 Earth's energy budget. In addition to data collection, open access to the data and data synthesis
988 products as well as coordinated international efforts are key to the continued monitoring of the ice
989 loss from the cryosphere and related energy uptake.
990
991 Sustained and improved observations to quantify Earth's changing energy inventory are also
992 critical to the development of improved physical models of the climate system, including both data
993 assimilation efforts that help us to understand past changes and predictions (Storto et al., 2019)
994 and climate models used to provide projections of future climate change (Eyring et al., 2019). For
995 example, atmospheric reanalyses have shown to be a valuable tool for investigating past changes
996 in the EEI (Allan et al., 2014) and ocean reanalyses have proven useful in estimating rates of ocean
997 heating on annual and sub-annual timescales by reducing observational noise (Trenberth et al.,
998 2016). Furthermore, both reanalyses and climate models can provide information to assess current
999 observing capabilities (Fujii et al., 2019) and improve uncertainty estimates in the different
1000 components of Earth's energy inventory (Allison et al., 2019). Future priorities for expanding the
1001 observing system to improve future estimates of EEI should be cognizant of the expected evolution
1002 of the climate change signal, drawing on evidence from observations, models and theory
1003 (Meyssignac et al., 2019; Palmer et al., 2019).
1004
1005 A continuous effort to regularly update the Earth heat inventory is important to quantify how much
1006 and where heat accumulated from climate change is stored in the climate system. The Earth heat
1007 inventory crosses multi-disciplinary boundaries, and calls for the inclusion of new science
1008 knowledge from the different disciplines involved, including the evolution of climate observing
1009 systems and associated data products, uncertainty evaluations and processing tools. The results
1010 provide indications that a redistribution and conversion of energy in the form of heat is taking
1011 place in the different components of the Earth system, particularly within the ocean, and that EEI
1012 has increased over the past decade. The outcomes have further demonstrated how we are able to
1013 evolve our estimates for the Earth heat inventory while bringing together different expertise and
1014 major climate science advancements through a concerted international effort. All of these

1015   component estimates are at the leading edge of climate science. Their union has provided a new
1016   and unique insight on the inventory of heat in the Earth system, its evolution over time, as well as
1017   a revision of the absolute values. The data product of this effort is made available and can be thus
1018   used for model validation purposes.

1019

1020   This study has demonstrated the unique value of such a concerted international effort, and we thus
1021   call for a regular evaluation of the Earth heat inventory. This first attempt presented here has been
1022   focused on the global area average only, and evolving into regional heat storage and redistribution,
1023   the inclusion of various time-scales (e.g. seasonal, year-to-year), and other climate study tools (e.g.
1024   indirect methods, ocean reanalyses) would be an important asset of this much needed regular
1025   international framework for the Earth heat inventory. This would also respond directly to the
1026   request of GCOS to establish the observational requirements needed to monitor the Earth's cycles
1027   and the global energy budget. The outcome of this study will therefore directly feed into GCOS'
1028   assessment of the status of the global climate observing system due in 2021 which is the basis for
1029   the next implementation plan. These identified observation requirements will guide the
1030   development of the next generation of in-situ and satellite global climate observations by all
1031   national meteorological services and space agencies and other oceanic and terrestrial networks.

1032

1033

1034

1035   **Data availability:** The time series of the Earth heat inventory are published at DKRZ
1036   (https://www.dkrz.de/) under the doi: https://doi.org/10.26050/WDCC/GCOS_EHI_EXP_v2 (von
1037   Schuckmann et al., 2020). The data contain an updated international assessment of ocean warming
1038   estimates, and new and updated estimates of heat gain in the atmosphere, cryosphere and land over
1039   the period 1960-2018. This published dataset has been used to build the basis for Figure 6 of this
1040   manuscript. The ocean warming estimate is based on an international assessment of 15 different
1041   in situ data-based ocean products as presented in section 1. The new estimate of the atmospheric
1042   heat content is fully described in section 2, and is backboned on a combined use of atmospheric
1043   reanalyses, multi-satellite data and radiosonde records, and microwave sounding techniques. The
1044   land heat storage time series as presented in section 3 relies on borehole data. The heat available
1045   to account for cryosphere loss is presented in section 4, and is based on a combined use of model
1046   results and observations to obtain estimates of major cryosphere components such as polar ice
1047   sheets, Arctic sea-ice and glaciers.

1048
1049
1050
1051
1052
1053
1054

GCOS Earth heat inventory team: Author contributions

Coordination: Karina von Schuckmann[1], Lijing Cheng[2,28], Matthew D. Palmer[3], Caterina Tassone[5], Valentin Aich[5]

Ocean: Karina von Schuckmann[1], Lijing Cheng[2,28], Tim Boyer[8], Damien Desbruyères[9], Catia Domingues[10,11], John Gilson[13], Masayoshi Ishii[16], Gregory C. Johnson[17], Rachel E. Killick[3], Brian A. King[10], Nicolas Kolodziejczyk[18], John Lyman[17], Maeva Monier[20], Didier Paolo Monselesan[21], Sarah Purkey[6], Dean Roemmich[6], Susan E. Wijffels[21,26]

Atmosphere: Gottfried Kirchengast[14], Maximilian Gorfer[14], Andrea K. Steiner[14], Michael Mayer[15,29], Leopold Haimberger[15]

Land: Almudena García-García[7], Francisco José Cuesta-Valero[7,27], Hugo Beltrami[7], Sonia I. Seneviratne[23], Pierre Gentine[12]

Cryosphere: Fiammetta Straneo[6], Susheel Adusumilli[6], Donald A. Slater[6], Mary-Louise Timmermans[25], Ben Marzeion[19], Axel Schweiger[22], Andrew Shepherd[24]

Earth energy inventory: all authors, with specific contributions from Karina von Schuckmann[1], Almudena García-García[7], Francisco José Cuesta-Valero[7,27], James Hansen[4], Maeva Monier[19]

Conclusion: all authors, with specific contributions from Karina von Schuckmann[1], James Hansen[4], Caterina Tassone[5], Valentin Aich[5], Lijing Cheng[2,28], Matthew D. Palmer[3], Gottfried Kirchengast[14], Andrea K. Steiner[14], Almudena García-García[7], Francisco José Cuesta-Valero[7,27], Hugo Beltrami[7], Fiammetta Straneo[6]

[1]Mercator Ocean International, France
[2]Institute of Atmospheric Physics, Chinese Academy of Sciences, China
[3]Met Office Hadley Centre, UK
[4]Columbia University Earth Institute, USA
[5]WMO/GCOS, Switzerland
[6]Scripps Institution of Oceanography, UCSD, San Diego, CA, USA
[7]Climate & Atmospheric Sciences Institute, St. Francis Xavier University, NS, Canada
[8]NOAA's National Centers for Environmental Information
[9]Ifremer, University of Brest, CNRS, IRD, Laboratoire d'Océanographie Physique et Spatiale, France
[10]National Oceanographic Centre, UK
[11]ARC Centre of Excellence for Climate Extremes, University of Tasmania, Hobart, Tasmania, Australia
[12]Earth and Environmental Engineering in the School of Engineering and Applied Sciences, Columbia University, USA
[13]University of California, USA
[14]Wegener Center for Climate and Global Change and Institute of Physics, University of Graz, Austria
[15]Department of Meteorology and Geophysics, University of Vienna, Austria

[16]Department of Atmosphere, Ocean and Earth System Modeling Research, Meteorological Research Institute, Japan
[17]NOAA, Pacific Marine Environmental Laboratory, USA
[18]University of Brest, CNRS, IRD, Ifremer, Laboratoire d'Océanographie Physique et Spatiale, IUEM, France
[19]Institute of Geography and MARUM-Center for Marine Environmental Sciences, University of Bremen, Germany
[20]CELAD/Mercator Ocean International, France
[21]CSIRO Oceans and Atmosphere, Hobart, Tasmania, Australia
[22]Polar Science Center, Applied Physics Laboratory, University of Washington, Seattle, USA
[23]Institute for Atmospheric and Climate Science, ETH, Switzerland
[24]Center for Polar Observation and Modeling, University of Leeds, UK
[25]Department of Earth and Planetary Sciences, Yale University, New Haven, USA
[26]Woods Hole Oceanographic Institution, Massachusetts, United States
[27]Environmental Sciences Program, Memorial University of Newfoundland, NL, Canada
[28]Center for Ocean Mega-Science, Chinese Academy of Sciences, Qingdao, China, 266071
[29]European Centre for Medium-Range Weather Forecasts, Reading, UK

Acknowledgements:

This research benefited from long-term attention by GCOS and builds on initial work carried out under the WCRP core projects CLIVAR, GEWEX, CliC and SPARC.

MDP and REK were supported by the Met Office Hadley Centre Climate Programme funded by the BEIS and Defra.

Ocean: PMEL contribution number 5053; Funding: CMD was supported by an ARC Future Fellowship (FT130101532). L.Cheng is supported by Key Deployment Project of Centre for Ocean Mega-Research of Science, CAS (COMS2019Q01).

Atmosphere: The authors express their gratitude to SPARC for supporting this activity under sponsorship of the WCRP. M. Gorfer was supported by WEGC atmospheric remote sensing and climate system research group young scientist funds. M. Mayer was supported by Austrian Science Fund project P33177. We acknowledge the WEGC EOPAC team for providing the OPSv5.6 RO data (available online at https://doi.org/10.25364/WEGC/OPS5.6:2019.1) as well as quality-processed Vaisala RS data, UCAR/CDAAC (Boulder, CO, USA) for access to RO phase and orbit data, RSS (Santa Rosa, CA, USA) for providing MSU V4.0 data, ECMWF (Reading, UK) for access to operational analysis and forecast data, ERA5 reanalysis data, and RS data from the ERA-Interim archive, JMA (Tokyo, Japan) for provision of the JRA55 and JRA55C reanalysis data, and NASA GMAO (Greenbelt, MD, USA) for access of the MERRA-2 reanalysis data.

Land: This work was supported by grants from the National Sciences and Engineering Research Council of Canada Discovery Grant (NSERC DG 140576948) and the Canada Research Chairs Program (CRC 230687) to H. Beltrami. Almudena García-García and Francisco José Cuesta-Valero are funded by Beltrami's CRC program, the School of Graduate Studies at Memorial University of Newfoundland and the Research Office at St. Francis Xavier University

1142 Ice: This work was supported by CliC (Climate and Cryosphere Project of the World Climate Research
1143 Program). FS acknowledges support by NSF OCE 1657601. SA was supported by the NASA grant
1144 80NSSC18K1424.

1145

1146 We also would like to thank Marianne Nail (https://girlsmakesense.com/) for her support to the graphical
1147 development of Fig. 7 and 8.

1148

1149

1150

References

1152 Abraham, J. P., Baringer, M., Bindoff, N. L., Boyer, T., Cheng, L. J., Church, J. A., Conroy, J. L., Domingues, C.
1153   M., Fasullo, J. T., Gilson, J., Goni, G., Good, S. A., Gorman, J. M., Gouretski, V., Ishii, M., Johnson, G. C.,
1154   Kizu, S., Lyman, J. M., Macdonald, A. M., … Willis, J. K. (2013). A review of global ocean temperature
1155   observations: Implications for ocean heat content estimates and climate change. *Reviews of Geophysics*, *51*(3),
1156   450–483. https://doi.org/10.1002/rog.20022
1157 Adusumilli, S., Fricker, H. A., Medley, B., Padman, L., & Siegfried, M. R. (2019). Multi-year variability in ocean-
1158   driven melting of Antarctica's ice shelves. *Nature Geoscience*, under review.
1159 Allan, R. P., Liu, C., Loeb, N. G., Palmer, M. D., Roberts, M., Smith, D., & Vidale, P.-L. (2014). Changes in global
1160   net radiative imbalance 1985-2012 (I10, trans.). *Geophysical Research Letters*, *41*(15), 5588–5597.
1161   https://doi.org/10.1002/2014GL060962
1162 Allison, L. C., Roberts, C. D., Palmer, M. D., Hermanson, L., Killick, R. E., Rayner, N. A., Smith, D. M., &
1163   Andrews, M. B. (2019). Towards quantifying uncertainty in ocean heat content changes using synthetic
1164   profiles. *Environmental Research Letters*, *14*(8), 084037. https://doi.org/10.1088/1748-9326/ab2b0b
1165 Angerer, B., Ladstädter, F., Scherllin-Pirscher, B., Schwärz, M., Steiner, A. K., Foelsche, U., & Kirchengast, G.
1166   (2017). Quality aspects of the Wegener Center multi-satellite GPS radio occultation record OPSv5.6. *Atmos.
1167   Meas. Tech.*, *10*(12), 4845–4863. https://doi.org/10.5194/amt-10-4845-2017
1168 Baggenstos, D., Häberli, M., Schmitt, J., Shackleton, S. A., Birner, B., Severinghaus, J. P., Kellerhals, T., & Fischer,
1169   H. (2019). Earth's radiative imbalance from the Last Glacial Maximum to the present. *Proceedings of the
1170   National Academy of Sciences*, *116*(30), 14881. https://doi.org/10.1073/pnas.1905447116
1171 Bailey, V. L., Pries, C. H., & Lajtha, K. (2019). What do we know about soil carbon destabilization? *Environmental
1172   Research Letters*, *14*(8), 083004. https://doi.org/10.1088/1748-9326/ab2c11
1173 Bamber, J. L., Westaway, R. M., Marzeion, B., & Wouters, B. (2018). The land ice contribution to sea level during
1174   the satellite era. *Environmental Research Letters*, *13*(6), 063008. https://doi.org/10.1088/1748-9326/aac2f0
1175 Barkaoui, A. E., Correia, A., Zarhloule, Y., Rimi, A., Carneiro, J., Boughriba, M., & Verdoya, M. (2013).
1176   Reconstruction of remote climate change from borehole temperature measurement in the eastern part of
1177   Morocco. *Climatic Change*, *118*(2), 431–441. https://doi.org/10.1007/s10584-012-0638-7
1178 Beck, A. E. (1977). Climatically perturbed temperature gradients and their effect on regional and continental heat-
1179   flow means. *Tectonophysics*, *41*(1), 17–39. https://doi.org/https://doi.org/10.1016/0040-1951(77)90178-0
1180 Beltrami, H. (2001). Surface heat flux histories from inversion of geothermal data: Energy balance at the Earth's
1181   surface. *Journal of Geophysical Research: Solid Earth*, *106*(B10), 21979–21993.
1182   https://doi.org/10.1029/2000JB000065
1183 Beltrami, H. (2002a). Earth's Long-Term Memory. *Science*, *297*(5579), 206.
1184   https://doi.org/10.1126/science.1074027
1185 Beltrami, H. (2002b). Climate from borehole data: Energy fluxes and temperatures since 1500. *Geophysical
1186   Research Letters*, *29*(23), 26-1-26–4. https://doi.org/10.1029/2002GL015702
1187 Beltrami, H., & Bourlon, E. (2004). Ground warming patterns in the Northern Hemisphere during the last five
1188   centuries. *Earth and Planetary Science Letters*, *227*(3), 169–177.
1189   https://doi.org/https://doi.org/10.1016/j.epsl.2004.09.014
1190 Beltrami, H., Bourlon, E., Kellman, L., & González-Rouco, J. F. (2006). Spatial patterns of ground heat gain in the
1191   Northern Hemisphere. *Geophysical Research Letters*, *33*(6). https://doi.org/10.1029/2006GL025676
1192 Beltrami, H., Matharoo, G. S., & Smerdon, J. E. (2015). Impact of borehole depths on reconstructed estimates of

1193   ground surface temperature histories and energy storage. *Journal of Geophysical Research: Earth Surface*,
1194   *120*(5), 763–778. https://doi.org/10.1002/2014JF003382

1195   Beltrami, H., Matharoo, G. S., Smerdon, J. E., Illanes, L., & Tarasov, L. (2017). Impacts of the Last Glacial Cycle
1196   on ground surface temperature reconstructions over the last millennium. *Geophysical Research Letters*, *44*(1),
1197   355–364. https://doi.org/10.1002/2016GL071317

1198   Beltrami, H., Smerdon, J. E., Pollack, H. N., & Huang, S. (2002). Continental heat gain in the global climate system.
1199   *Geophysical Research Letters*, *29*(8), 8-1-8–3. https://doi.org/10.1029/2001GL014310

1200   Bense, V. F., & Kooi, H. (2004). Temporal and spatial variations of shallow subsurface temperature as a record of
1201   lateral variations in groundwater flow. *Journal of Geophysical Research: Solid Earth*, *109*(B4).
1202   https://doi.org/10.1029/2003JB002782

1203   Berrisford, P., Kållberg, P., Kobayashi, S., Dee, D., Uppala, S., Simmons, A. J., Poli, P., & Sato, H. (2011).
1204   Atmospheric conservation properties in ERA-Interim. *Quarterly Journal of the Royal Meteorological Society*,
1205   *137*(659), 1381–1399. https://doi.org/10.1002/qj.864

1206   Bindoff, N. L., Cheung, W. W. L., & Kairo, J. G. (2019). Changing Oean, Marine Ecosystems, and Dependent
1207   Communities. In H. O. Pörtner, D. C. Roberts, V. Masson-Delmotte, P. Zhai, M. Tignor, E. Poloczanska, K.
1208   Mintenbeck, A. Alegría, M. Nicolai, A. Okem, J. Petzold, B. Rama, & N. M. Weyer (Eds.), *Special Report:*
1209   *The Ocean and Cryosphere in a Changing Climate Summary for Policymakers* (pp. 447–587). in press.
1210   https://doi.org/https://www.ipcc.ch/report/srocc/

1211   Blunden, J. and Arndt, D. S. (2019). State of the Climate in 2019. Bulletin of the American Meteorological Society,
1212   100(9), Si–S305, doi:10.1175/2019BAMSStateoftheClimate.1.

1213   Bopp, L., Resplandy, L., Orr, J. C., Doney, S. C., Dunne, J. P., Gehlen, M., Halloran, P., Heinze, C., Ilyina, T.,
1214   Séférian, R., Tjiputra, J., & Vichi, M. (2013). Multiple stressors of ocean ecosystems in the 21st century:
1215   projections with CMIP5 models. *Biogeosciences*, *10*(10), 6225–6245. https://doi.org/10.5194/bg-10-6225-
1216   2013

1217   Boyer, T., Domingues, C. M., Good, S. A., Johnson, G. C., Lyman, J. M., Ishii, M., Gouretski, V., Willis, J. K.,
1218   Antonov, J., Wijffels, S., Church, J. A., Cowley, R., & Bindoff, N. L. (2016). Sensitivity of Global Upper-
1219   Ocean Heat Content Estimates to Mapping Methods, XBT Bias Corrections, and Baseline Climatologies.
1220   *Journal of Climate*, *29*(13), 4817–4842. https://doi.org/10.1175/JCLI-D-15-0801.1

1221   Breitburg, D., Levin, L. A., Oschlies, A., Grégoire, M., Chavez, F. P., Conley, D. J., Garçon, V., Gilbert, D.,
1222   Gutiérrez, D., Isensee, K., Jacinto, G. S., Limburg, K. E., Montes, I., Naqvi, S. W. A., Pitcher, G. C., Rabalais,
1223   N. N., Roman, M. R., Rose, K. A., Seibel, B. A., … Zhang, J. (2018). Declining oxygen in the global ocean
1224   and coastal waters. *Science*, *359*(6371), eaam7240. https://doi.org/10.1126/science.aam7240

1225   Cabanes, C., Grouazel, A., Von Schuckmann, K., Hamon, M., Turpin, V., Coatanoan, C., Paris, F., Guinehut, S.,
1226   Boone, C., Ferry, N., De Boyer Montégut, C., Carval, T., Reverdin, G., Pouliquen, S., & Le Traon, P. Y.
1227   (2013). The CORA dataset: Validation and diagnostics of in-situ ocean temperature and salinity
1228   measurements. *Ocean Science*, *9*(1), 1–18. https://doi.org/10.5194/os-9-1-2013

1229   Cermak, V. (1971). Underground temperature and inferred climatic temperature of the past millenium.
1230   *Palaeogeography, Palaeoclimatology, Palaeoecology*, *10*(1), 1–19. https://doi.org/10.1016/0031-
1231   0182(71)90043-5

1232   Cheng, L., Trenberth, K., Fasullo, J., Boyer, T., Abraham, J., von Schuckmann, K., & Zhou, J. (2017). Taking the
1233   Pulse of the Planet. *Eos, Transactions American Geophysical Union*, *98*(1).
1234   https://doi.org/10.1029/2017EO081839

1235   Cheng, L, Trenberth, K. E., Palmer, M. D., Zhu, J., & Abraham, J. P. (2016). Observed and simulated full-depth
1236   ocean heat-content changes for 1970–2005. *Ocean Sci.*, *12*(4), 925–935. https://doi.org/10.5194/os-12-925-
1237   2016

1238   Cheng, Lijing, Abraham, J., Hausfather, Z., & Trenberth, K. E. (2019). How fast are the oceans warming? *Science*,
1239   *363*(6423), 128. https://doi.org/10.1126/science.aav7619

1240   Cheng, Lijing, Trenberth, K. E., Fasullo, J., Boyer, T., Abraham, J., & Zhu, J. (2017). Improved estimates of ocean
1241   heat content from 1960 to 2015. *Science Advances*, *3*(3), e1601545. https://doi.org/10.1126/sciadv.1601545

1242   Cheng, Lijing, Trenberth, K. E., Fasullo, J. T., Mayer, M., Balmaseda, M., & Zhu, J. (2019). Evolution of ocean heat
1243   content related to ENSO. *Journal of Climate*, *32*(12), 3529–3556. https://doi.org/10.1175/JCLI-D-18-0607.1

1244   Chiodo, G., & Haimberger, L. (2010). Interannual changes in mass consistent energy budgets from ERA-Interim and
1245   satellite data. *Journal of Geophysical Research: Atmospheres*, *115*(D2).
1246   https://doi.org/10.1029/2009JD012049

1247   Chouinard, C, & Mareschal, J.-C. (2007). Selection of borehole temperature depth profiles for regional climate
1248   reconstructions. *Clim. Past*, *3*(2), 297–313. https://doi.org/10.5194/cp-3-297-2007

Chouinard, Christian, & Mareschal, J.-C. (2009). Ground surface temperature history in southern Canada: Temperatures at the base of the Laurentide ice sheet and during the Holocene. *Earth and Planetary Science Letters*, *277*(1–2), 280–289. https://doi.org/10.1016/j.epsl.2008.10.026

Ciais, P., Sabine, C., Bala, G., Bopp, L., Brovkin, V., Canadell, J., Chhabra, A., DeFries, R., Galloway, J., Heimann, M., Jones, C., Quéré, C. Le, Myneni, R. B., Piao, S., & Thornton, P. (2013). The physical science basis. Contribution of working group I to the fifth assessment report of the intergovernmental panel on climate change. *Change, IPCC Climate*, 465–570. https://doi.org/10.1017/CBO9781107415324.015

Clark, P. U., Shakun, J. D., Marcott, S. A., Mix, A. C., Eby, M., Kulp, S., Levermann, A., Milne, G. A., Pfister, P. L., Santer, B. D., Schrag, D. P., Solomon, S., Stocker, T. F., Strauss, B. H., Weaver, A. J., Winkelmann, R., Archer, D., Bard, E., Goldner, A., … Plattner, G.-K. (2016). Consequences of twenty-first-century policy for multi-millennial climate and sea-level change. *Nature Climate Change*, *6*(4), 360–369. https://doi.org/10.1038/nclimate2923

Cohen, J., Screen, J. A., Furtado, J. C., Barlow, M., Whittleston, D., Coumou, D., Francis, J., Dethloff, K., Entekhabi, D., Overland, J., & Jones, J. (2014). Recent Arctic amplification and extreme mid-latitude weather. *Nature Geoscience*, *7*(9), 627–637. https://doi.org/10.1038/ngeo2234

Cook, A. J., & Vaughan, D. G. (2010). Overview of areal changes of the ice shelves on the Antarctic Peninsula over the past 50 years. *The Cryosphere*, *4*(1), 77–98. https://doi.org/10.5194/tc-4-77-2010

Coumou, D., Di Capua, G., Vavrus, S., Wang, L., & Wang, S. (2018). The influence of Arctic amplification on mid-latitude summer circulation. *Nature Communications*, *9*(1), 2959. https://doi.org/10.1038/s41467-018-05256-8

Cuesta-Valero, F J, García-García, A., Beltrami, H., González-Rouco, J. F., & García-Bustamante, E. (2020). Long-Term Global Ground Heat Flux and Continental Heat Storage from Geothermal Data. *Clim. Past Discuss.*, *2020*, 1–27. https://doi.org/10.5194/cp-2020-65

Cuesta-Valero, F J, García-García, A., Beltrami, H., Zorita, E., & Jaume-Santero, F. (2019). Long-term Surface Temperature (LoST) database as a complement for GCM preindustrial simulations. *Clim. Past*, *15*(3), 1099–1111. https://doi.org/10.5194/cp-15-1099-2019

Cuesta-Valero, Francisco José, García-García, A., Beltrami, H., & Smerdon, J. E. (2016). First assessment of continental energy storage in CMIP5 simulations. *Geophysical Research Letters*, *43*(10), 5326–5335. https://doi.org/10.1002/2016GL068496

Davis, M. G., Harris, R. N., & Chapman, D. S. (2010). Repeat temperature measurements in boreholes from northwestern Utah link ground and air temperature changes at the decadal time scale. *Journal of Geophysical Research: Solid Earth*, *115*(B5). https://doi.org/10.1029/2009JB006875

Demezhko, D. Y., & Gornostaeva, A. A. (2015). Late Pleistocene–Holocene ground surface heat flux changes reconstructed from borehole temperature data (the Urals, Russia). *Clim. Past*, *11*(4), 647–652. https://doi.org/10.5194/cp-11-647-2015

Desbruyères, D. G., Purkey, S. G., McDonagh, E. L., Johnson, G. C., & King, B. A. (2016). Deep and abyssal ocean warming from 35 years of repeat hydrography. *Geophysical Research Letters*, *43*(19), 10, 310–356, 365. https://doi.org/10.1002/2016GL070413

Desbruyères, D., McDonagh, E. L., King, B. A., & Thierry, V. (2017). Global and Full-Depth Ocean Temperature Trends during the Early Twenty-First Century from Argo and Repeat Hydrography. *Journal of Climate*, *30*(6), 1985–1997. https://doi.org/10.1175/JCLI-D-16-0396.1

Dieng, H. B., Cazenave, A., Meyssignac, B., & Ablain, M. (2017). New estimate of the current rate of sea level rise from a sea level budget approach. *Geophysical Research Letters*, *44*(8), 3744–3751. https://doi.org/10.1002/2017GL073308

Eyring, V., Cox, P. M., Flato, G. M., Gleckler, P. J., Abramowitz, G., Caldwell, P., Collins, W. D., Gier, B. K., Hall, A. D., Hoffman, F. M., Hurtt, G. C., Jahn, A., Jones, C. D., Klein, S. A., Krasting, J. P., Kwiatkowski, L., Lorenz, R., Maloney, E., Meehl, G. A., … Williamson, M. S. (2019). Taking climate model evaluation to the next level. *Nature Climate Change*, *9*(2), 102–110. https://doi.org/10.1038/s41558-018-0355-y

Fischer, E. M., & Knutti, R. (2016). Observed heavy precipitation increase confirms theory and early models. *Nature Climate Change*, *6*(11), 986–991. https://doi.org/10.1038/nclimate3110

Friedlingstein, P., Jones, M. W., O'Sullivan, M., Andrew, R. M., Hauck, J., Peters, G. P., Peters, W., Pongratz, J., Sitch, S., Le Quéré, C., Bakker, D. C. E., Canadell, J. G., Ciais, P., Jackson, R. B., Anthoni, P., Barbero, L., Bastos, A., Bastrikov, V., Becker, M., Bopp, L., Buitenhuis, E., Chandra, N., Chevallier, F., Chini, L. P., Currie, K. I., Feely, R. A., Gehlen, M., Gilfillan, D., Gkritzalis, T., Goll, D. S., Gruber, N., Gutekunst, S., Harris, I., Haverd, V., Houghton, R. A., Hurtt, G., Ilyina, T., Jain, A. K., Joetzjer, E., Kaplan, J. O., Kato, E., Klein Goldewijk, K., Korsbakken, J. I., Landschützer, P., Lauvset, S. K., Lefèvre, N., Lenton, A., Lienert, S., Lombardozzi, D., Marland, G., McGuire, P. C., Melton, J. R., Metzl, N., Munro, D. R., Nabel, J. E. M. S.,

Nakaoka, S.-I., Neill, C., Omar, A. M., Ono, T., Peregon, A., Pierrot, D., Poulter, B., Rehder, G., Resplandy, L., Robertson, E., Rödenbeck, C., Séférian, R., Schwinger, J., Smith, N., Tans, P. P., Tian, H., Tilbrook, B., Tubiello, F. N., van der Werf, G. R., Wiltshire, A. J., and Zaehle, S.: Global Carbon Budget 2019, Earth Syst. Sci. Data, 11, 1783–1838, https://doi.org/10.5194/essd-11-1783-2019, 2019.

Frölicher, T. L., Fischer, E. M., & Gruber, N. (2018). Marine heatwaves under global warming. *Nature*, *560*(7718), 360–364. https://doi.org/10.1038/s41586-018-0383-9

Fu, Q., Solomon, S., Pahlavan, H. A., & Lin, P. (2019). Observed changes in Brewer–Dobson circulation for 1980–2018. *Environmental Research Letters*, *14*(11), 114026. https://doi.org/10.1088/1748-9326/ab4de7

Fujii, Y., Rémy, E., Zuo, H., Oke, P., Halliwell, G., Gasparin, F., Benkiran, M., Loose, N., Cummings, J., Xie, J., Xue, Y., Masuda, S., Smith, G. C., Balmaseda, M., Germineaud, C., Lea, D. J., Larnicol, G., Bertino, L., Bonaduce, A., … Usui, N. (2019). Observing System Evaluation Based on Ocean Data Assimilation and Prediction Systems: On-Going Challenges and a Future Vision for Designing and Supporting Ocean Observational Networks . In *Frontiers in Marine Science* (Vol. 6, p. 417). https://www.frontiersin.org/article/10.3389/fmars.2019.00417

Gaillard, F., Reynaud, T., Thierry, V., Kolodziejczyk, N., & von Schuckmann, K. (2016). In Situ–Based Reanalysis of the Global Ocean Temperature and Salinity with ISAS: Variability of the Heat Content and Steric Height. *Journal of Climate*, *29*(4), 1305–1323. https://doi.org/10.1175/JCLI-D-15-0028.1

García Molinos, J., Halpern, B. S., Schoeman, D. S., Brown, C. J., Kiessling, W., Moore, P. J., Pandolfi, J. M., Poloczanska, E. S., Richardson, A. J., & Burrows, M. T. (2016). Climate velocity and the future global redistribution of marine biodiversity. *Nature Climate Change*, *6*(1), 83–88. https://doi.org/10.1038/nclimate2769

García-García, A, Cuesta-Valero, F. J., Beltrami, H., & Smerdon, J. E. (2016). Simulation of air and ground temperatures in PMIP3/CMIP5 last millennium simulations: implications for climate reconstructions from borehole temperature profiles. *Environmental Research Letters*, *11*(4), 044022. https://doi.org/10.1088/1748-9326/11/4/044022

García-García, Almudena, Cuesta-Valero, F. J., Beltrami, H., & Smerdon, J. E. (2019). Characterization of Air and Ground Temperature Relationships within the CMIP5 Historical and Future Climate Simulations. *Journal of Geophysical Research: Atmospheres*, *124*(7), 3903–3929. https://doi.org/10.1029/2018JD030117

Gardner, A. S., Moholdt, G., Cogley, J. G., Wouters, B., Arendt, A. A., Wahr, J., Berthier, E., Hock, R., Pfeffer, W. T., Kaser, G., Ligtenberg, S. R. M., Bolch, T., Sharp, M. J., Hagen, J. O., van den Broeke, M. R., & Paul, F. (2013). A Reconciled Estimate of Glacier Contributions to Sea Level Rise: 2003 to 2009. *Science*, *340*(6134), 852. https://doi.org/10.1126/science.1234532

Gattuso, J.-P., Magnan, A., Billé, R., Cheung, W. W. L., Howes, E. L., Joos, F., Allemand, D., Bopp, L., Cooley, S. R., Eakin, C. M., Hoegh-Guldberg, O., Kelly, R. P., Pörtner, H.-O., Rogers, A. D., Baxter, J. M., Laffoley, D., Osborn, D., Rankovic, A., Rochette, J., … Turley, C. (2015). Contrasting futures for ocean and society from different anthropogenic CO₂ emissions scenarios. *Science*, *349*(6243), aac4722. https://doi.org/10.1126/science.aac4722

GCOS. (2016). *The Global Observing System for Climate: Implementation needs*. https://doi.org/https://doi.org/DOI: 10.13140/RG.2.2.23178.26566

Gelaro, R., McCarty, W., Suárez, M. J., Todling, R., Molod, A., Takacs, L., Randles, C. A., Darmenov, A., Bosilovich, M. G., Reichle, R., Wargan, K., Coy, L., Cullather, R., Draper, C., Akella, S., Buchard, V., Conaty, A., da Silva, A. M., Gu, W., … Zhao, B. (2017). The Modern-Era Retrospective Analysis for Research and Applications, Version 2 (MERRA-2). *Journal of Climate*, *30*(14), 5419–5454. https://doi.org/10.1175/JCLI-D-16-0758.1

Gentine, P., Garcia-Garcia, A., Meier, R., Cuesta-Valero, F., Hugo., B., Davin, E. L., & Seneviratne, S. I. (2020). Large recent continental heat storage. *Nature*, *under revi*.

Gleckler, P., Durack, P., Ronald, S., Johnson, G., & Forest, C. (2016). Industrial-era global ocean heat uptake doubles in recent decades. *Nature Climate Change*, *6*. https://doi.org/10.1038/nclimate2915

Goni, G. J., Sprintall, J., Bringas, F., Cheng, L., Cirano, M., Dong, S., Domingues, R., Goes, M., Lopez, H., Morrow, R., Rivero, U., Rossby, T., Todd, R. E., Trinanes, J., Zilberman, N., Baringer, M., Boyer, T., Cowley, R., Domingues, C. M., … Volkov, D. (2019). More Than 50 Years of Successful Continuous Temperature Section Measurements by the Global Expendable Bathythermograph Network, Its Integrability, Societal Benefits, and Future. *Frontiers in Marine Science*, *6*, 452. https://www.frontiersin.org/article/10.3389/fmars.2019.00452

González-Rouco, J. F., Beltrami, H., Zorita, E., & Stevens, M. B. (2009). Borehole climatology: a discussion based on contributions from climate modeling. *Clim. Past*, *5*(1), 97–127. https://doi.org/10.5194/cp-5-97-2009

González-Rouco, J. F., Beltrami, H., Zorita, E., & von Storch, H. (2006). Simulation and inversion of borehole temperature profiles in surrogate climates: Spatial distribution and surface coupling. *Geophysical Research Letters*, *33*(1). https://doi.org/10.1029/2005GL024693

Good, S. A., Martin, M. J., & Rayner, N. A. (2013). EN4: Quality controlled ocean temperature and salinity profiles and monthly objective analyses with uncertainty estimates. *Journal of Geophysical Research: Oceans*, *118*(12), 6704–6716. https://doi.org/10.1002/2013JC009067

Gouretski, V., & Cheng, L. (2020). Correction for Systematic Errors in the Global Dataset of Temperature Profiles from Mechanical Bathythermographs. *Journal of Atmospheric and Oceanic Technology*, *37*(5), 841–855. https://doi.org/10.1175/JTECH-D-19-0205.1

Gregory, J. M., & Andrews, T. (2016). Variation in climate sensitivity and feedback parameters during the historical period. *Geophysical Research Letters*, *43*(8), 3911–3920. https://doi.org/10.1002/2016GL068406

Gregory, J. M., Andrews, T., Ceppi, P., Mauritsen, T., & Webb, M. J. (2020). How accurately can the climate sensitivity to $\hbox{CO}_{2}$ $CO2$ be estimated from historical climate change? *Climate Dynamics*, *54*(1), 129–157. https://doi.org/10.1007/s00382-019-04991-y

Guinehut, S., Dhomps, A.-L., Larnicol, G., & Le Traon, P.-Y. (2012). High resolution 3-D temperature and salinity fields derived from in situ and satellite observations. *Ocean Sci.*, *8*(5), 845–857. https://doi.org/10.5194/os-8-845-2012

Hansen, J. (2005). Efficacy of climate forcings. *Journal of Geophysical Research*, *110*(D18), D18104. https://doi.org/10.1029/2005JD005776

Hansen, J, Sato, M., Kharecha, P., & von Schuckmann, K. (2011). Earth's energy imbalance and implications. *Atmos. Chem. Phys.*, *11*(24), 13421–13449. https://doi.org/10.5194/acp-11-13421-2011

Hansen, J, Sato, M., Kharecha, P., von Schuckmann, K., Beerling, D. J., Cao, J., Marcott, S., Masson-Delmotte, V., Prather, M. J., Rohling, E. J., Shakun, J., Smith, P., Lacis, A., Russell, G., & Ruedy, R. (2017). Young people's burden: requirement of negative CO2 emissions. *Earth Syst. Dynam.*, *8*(3), 577–616. https://doi.org/10.5194/esd-8-577-2017

Hansen, James, Nazarenko, L., Ruedy, R., Sato, M., Willis, J., Del Genio, A., Koch, D., Lacis, A., Lo, K., Menon, S., Novakov, T., Perlwitz, J., Russell, G., Schmidt, G. A., & Tausnev, N. (2005). Earth's Energy Imbalance: Confirmation and Implications. *Science*, *308*(5727), 1431 LP – 1435. https://doi.org/10.1126/science.1110252

Harris, R. N., & Chapman, D. S. (2001). Mid-latitude (30°–60° N) climatic warming inferred by combining borehole temperatures with surface air temperatures. *Geophysical Research Letters*, *28*(5), 747–750. https://doi.org/10.1029/2000GL012348

Hartmann, A., & Rath, V. (2005). Uncertainties and shortcomings of ground surface temperature histories derived from inversion of temperature logs. *Journal of Geophysics and Engineering*, *2*(4), 299–311. https://doi.org/10.1088/1742-2132/2/4/S02

Hermoso de Mendoza, I., Beltrami, H., MacDougall, A. H., & Mareschal, J.-C. (2018). Lower boundary conditions in Land Surface Models. Effects on the permafrost and the carbon pools. *Geosci. Model Dev. Discuss.*, *2018*, 1–34. https://doi.org/10.5194/gmd-2018-233

Hersbach, H., Rosnay, P. de, Bell, B., Schepers, D., Simmons, A., Soci, C., Abdalla, S., Alonso-Balmaseda, M., Balsamo, G., Bechtold, P., Berrisford, P., Bidlot, J.-R., de Boisséson, E., Bonavita, M., Browne, P., Buizza, R., Dahlgren, P., Dee, D., Dragani, R., … Zuo, H. (2018). Operational global reanalysis: progress, future directions and synergies with NWP. In *ERA Report Series* (ERA Report). https://www.ecmwf.int/node/18765

Hersbach, H., Bell, B., Berrisford, P., Hirahara, S., Horányi, A., Muñoz-Sabater, J., Nicolas, J., Peubey, C., Radu, R., Schepers, D., Simmons, A., Soci, C., Abdalla, S., Abellan, X., Balsamo, G., Bechtold, P., Biavati, G., Bidlot, J., Bonavita, M., Chiara, G. D., Dahlgren, P., Dee, D., Diamantakis, M., Dragani, R., Flemming, J., Forbes, R., Fuentes, M., Geer, A., Haimberger, L., Healy, S., Hogan, R. J., Hólm, E., Janisková, M., Keeley, S., Laloyaux, P., Lopez, P., Lupu, C., Radnoti, G., Rosnay, P. de, Rozum, I., Vamborg, F., Villaume, S. & Thépaut, J.-N. (2020). The ERA5 global reanalysis, Q. J. R. Meteorol. Soc.. https://doi.org/10.1002/qj.3803.

Hicks Pries, C. E., Castanha, C., Porras, R., & Torn, M. S. (2017). The whole-soil carbon flux in response to warming. *Science*, eaal1319. https://doi.org/10.1126/science.aal1319

Hoegh-Guldberg, O., et al. (2018). *Global Warming on Natural and Human Systems. In: Global Warming of 1.5°C. An IPCC Special Report on the impacts of global warming of 1.5°C above pre-industrial levels and related global greenhouse gas emission pathways, in the context of strengthening the.*

Hopcroft, P. O., Gallagher, K., & Pain, C. C. (2007). Inference of past climate from borehole temperature data using Bayesian Reversible Jump Markov chain Monte Carlo. *Geophysical Journal International*, *171*(3), 1430–1439. https://doi.org/10.1111/j.1365-246X.2007.03596.x

1417 Huang, S. (2006). 1851–2004 annual heat budget of the continental landmasses. *Geophysical Research Letters*,
1418   *33*(4). https://doi.org/10.1029/2005GL025300
1419 Huang, S., Pollack, H. N., & Shen, P.-Y. (2000). Temperature trends over the past five centuries reconstructed from
1420   borehole temperatures. *Nature*, *403*(6771), 756–758. https://doi.org/10.1038/35001556
1421 IPCC Special Report on the Ocean and Cryosphere in a Changing Climate. (2019). In H. O. Pörtner, D. C. Roberts,
1422   V. Masson-Delmotte, P. Zhai, M. Tignor, E. Poloczanska, K. Mintenbeck, A. Alegría, M. Nicolai, A. Okem, J.
1423   Petzold, B. Rama, & N. M. Weyer (Eds.), *IPCC Intergovernmental Panel on Climate Change: Geneva,*
1424   *Switzerland*. https://www.ipcc.ch/srocc/
1425 Ishii, M., Fukuda, Y., Hirahara, S., Yasui, S., Suzuki, T., & Sato, K. (2017). Accuracy of Global Upper Ocean Heat
1426   Content Estimation Expected from Present Observational Data Sets. *SOLA*, *13*, 163–167.
1427   https://doi.org/10.2151/sola.2017-030
1428 Jacobs, S. S., Giulivi, C. F., & Mele, P. A. (2002). Freshening of the Ross Sea During the Late 20th Century.
1429   *Science*, *297*(5580), 386. https://doi.org/10.1126/science.1069574
1430 Jaume-Santero, F., Pickler, C., Beltrami, H., & Mareschal, J.-C. (2016). North American regional climate
1431   reconstruction from ground surface temperature histories. *Clim. Past*, *12*(12), 2181–2194.
1432   https://doi.org/10.5194/cp-12-2181-2016
1433 Jeong, D. Il, Sushama, L., Diro, G. T., Khaliq, M. N., Beltrami, H., & Caya, D. (2016). Projected changes to high
1434   temperature events for Canada based on a regional climate model ensemble. *Climate Dynamics*, *46*(9), 3163–
1435   3180. https://doi.org/10.1007/s00382-015-2759-y
1436 Johnson, G.C., Lyman, J.M. , Boyer, T., Cheng, L., Domingues, C.M., Gilson, J., Ishii, M., Killick, R., Monselesan,
1437   D., Purkey, S.G., Wijffels, S. E. (2018). Ocean heat content [in State of the Climate in 2017]. *Bulletin of the*
1438   *American Meteorological Society*, *99*(8), S72–S77.
1439 Johnson, G. C., & Birnbaum, A. N. (2017). As El Niño builds, Pacific Warm Pool expands, ocean gains more heat.
1440   *Geophysical Research Letters*, *44*(1), 438–445. https://doi.org/10.1002/2016GL071767
1441 Johnson, G. C., Lyman, J. M., & Purkey, S. G. (2015). Informing Deep Argo Array Design Using Argo and Full-
1442   Depth Hydrographic Section Data*. *Journal of Atmospheric and Oceanic Technology*, *32*(11), 2187–2198.
1443   https://doi.org/10.1175/JTECH-D-15-0139.1
1444 Johnson, G. C., Purkey, S. G., Zilberman, N. V, & Roemmich, D. (2019). Deep Argo Quantifies Bottom Water
1445   Warming Rates in the Southwest Pacific Basin. *Geophysical Research Letters*, *46*(5), 2662–2669.
1446   https://doi.org/10.1029/2018GL081685
1447 King, B. A., Firing, E., & M.Joyce, T. (2001). Chapter 3.1 Shipboard observations during WOCE. *International*
1448   *Geophysics*, *77*, 99–122. https://doi.org/10.1016/S0074-6142(01)80114-5
1449 King, M. D., Howat, I. M., Jeong, S., Noh, M. J., Wouters, B., Noël, B., & van den Broeke, M. R. (2018). Seasonal
1450   to decadal variability in ice discharge from the Greenland Ice Sheet. *The Cryosphere*, *12*(12), 3813–3825.
1451   https://doi.org/10.5194/tc-12-3813-2018
1452 King, M.D., Howat, I.M., Candela, S.G. et al. Dynamic ice loss from the Greenland Ice Sheet driven by sustained
1453   glacier retreat. Commun Earth Environ 1, 1 (2020). https://doi.org/10.1038/s43247-020-0001-2
1454 Kirchengast, G., Ladstädter, F., Steiner, A. K., Gorfer, M., Lippl, F., & Angerer, B. (2019). *Climate trends and*
1455   *variability in atmosphere heat content and atmosphere-ocean heat exchanges: space geodesy is key.* (No.
1456   IUGG19-4651). https://www.czech-
1457   in.org/cmPortalV15/CM_W3_Searchable/iugg19/normal#!sessiondetails/0000119801_0
1458 Knutti, R., & Rugenstein, M. A. A. (2015). Feedbacks, climate sensitivity and the limits of linear models.
1459   *Philosophical Transactions of the Royal Society A: Mathematical, Physical and Engineering Sciences*,
1460   *373*(2054), 20150146. https://doi.org/10.1098/rsta.2015.0146
1461 Kobayashi, S., Ota, Y., Harada, Y., Ebita, A., Moriya, M., Onoda, H., Onogi, K., Kamahori, H., Kobayashi, C.,
1462   Endo, H., MiyaokaI, K., & Takahashi, K. (2015). The JRA-55 Reanalysis: General Specifications and Basic
1463   Characteristics. *Journal of the Meteorological Society of Japan. Ser. II*, *93*(1), 5–48.
1464   https://doi.org/10.2151/jmsj.2015-001
1465 Kuhlbrodt, T., & Gregory, J. M. (2012). Ocean heat uptake and its consequences for the magnitude of sea level rise
1466   and climate change. *Geophysical Research Letters*, *39*(18). https://doi.org/10.1029/2012GL052952
1467 Labe, Z., Magnusdottir, G., & Stern, H. (2018). Variability of Arctic Sea Ice Thickness Using PIOMAS and the
1468   CESM Large Ensemble. *Journal of Climate*, *31*(8), 3233–3247. https://doi.org/10.1175/JCLI-D-17-0436.1
1469 Lachenbruch, A. H., & Marshall, B. V. (1986). Changing Climate: Geothermal Evidence from Permafrost in the
1470   Alaskan Arctic. *Science*, *234*(4777), 689–696. www.jstor.org/stable/1697932
1471 Ladstädter, F., Steiner, A. K., Schwärz, M., & Kirchengast, G. (2015). Climate intercomparison of GPS radio
1472   occultation, RS90/92 radiosondes and GRUAN from 2002 to 2013. *Atmos. Meas. Tech.*, *8*(4), 1819–1834.

https://doi.org/10.5194/amt-8-1819-2015

Lane, A. C. (1923). Geotherms of Lake Superior Copper Country. *GSA Bulletin*, *34*(4), 703–720. https://doi.org/10.1130/GSAB-34-703

Laxon, S. W., Giles, K. A., Ridout, A. L., Wingham, D. J., Willatt, R., Cullen, R., Kwok, R., Schweiger, A., Zhang, J., Haas, C., Hendricks, S., Krishfield, R., Kurtz, N., Farrell, S., & Davidson, M. (2013). CryoSat-2 estimates of Arctic sea ice thickness and volume. *Geophysical Research Letters*, *40*(4), 732–737. https://doi.org/10.1002/grl.50193

Leifeld, J., Wüst-Galley, C., & Page, S. (2019). Intact and managed peatland soils as a source and sink of GHGs from 1850 to 2100. *Nature Climate Change*, *9*(12), 945–947. https://doi.org/10.1038/s41558-019-0615-5

Lembo, V., Folini, D., Wild, M., & Lionello, P. (2019). Inter-hemispheric differences in energy budgets and cross-equatorial transport anomalies during the 20th century. *Climate Dynamics*, *53*(1), 115–135. https://doi.org/10.1007/s00382-018-4572-x

Lenton, T. M. (2011). Early warning of climate tipping points. *Nature Climate Change*, *1*(4), 201–209. https://doi.org/10.1038/nclimate1143

Lenton, T. M., Held, H., Kriegler, E., Hall, J. W., Lucht, W., Rahmstorf, S., & Schellnhuber, H. J. (2008). Tipping elements in the Earth's climate system. *Proceedings of the National Academy of Sciences of the United States of America*, *105*(6), 1786–1793. https://doi.org/10.1073/pnas.0705414105

Lenton, T., Rockström, J., Gaffney, O., Rahmstorf, S., Richardson, K., Steffen, W., & Schellnhuber, H. (2019). Climate tipping points — too risky to bet against. *Nature*, *575*, 592–595. https://doi.org/10.1038/d41586-019-03595-0

Levitus, S., Antonov, J. I., Boyer, T. P., Baranova, O. K., Garcia, H. E., Locarnini, R. A., Mishonov, A. V, Reagan, J. R., Seidov, D., Yarosh, E. S., & Zweng, M. M. (2012). World ocean heat content and thermosteric sea level change (0–2000 m), 1955–2010. *Geophysical Research Letters*, *39*(10). https://doi.org/10.1029/2012GL051106

Ligtenberg, S. R. M., Kuipers Munneke, P., Noël, B. P. Y., & van den Broeke, M. R. (2018). Brief communication: Improved simulation of the present-day Greenland firn layer (1960–2016). *The Cryosphere*, *12*(5), 1643–1649. https://doi.org/10.5194/tc-12-1643-2018

Llovel, W., Willis, J. K., Landerer, F. W., & Fukumori, I. (2014). Deep-ocean contribution to sea level and energy budget not detectable over the past decade. *Nature Climate Change*, *4*(11), 1031–1035. https://doi.org/10.1038/nclimate2387

Loeb, N. G., Lyman, J. M., Johnson, G. C., Allan, R. P., Doelling, D. R., Wong, T., Soden, B. J., & Stephens, G. L. (2012). Observed changes in top-of-the-atmosphere radiation and upper-ocean heating consistent within uncertainty. *Nature Geoscience*, *5*(2), 110–113. https://doi.org/10.1038/ngeo1375

Lyman, J. M., & Johnson, G. C. (2013). Estimating Global Ocean Heat Content Changes in the Upper 1800 m since 1950 and the Influence of Climatology Choice. *Journal of Climate*, *27*(5), 1945–1957. https://doi.org/10.1175/JCLI-D-12-00752.1

MacDougall, A. H., Avis, C. A., & Weaver, A. J. (2012). Significant contribution to climate warming from the permafrost carbon feedback. *Nature Geoscience*, *5*(10), 719–721. https://doi.org/10.1038/ngeo1573

MacDougall, A. H., Beltrami, H., González-Rouco, J. F., Stevens, M. B., & Bourlon, E. (2010). Comparison of observed and general circulation model derived continental subsurface heat flux in the Northern Hemisphere. *Journal of Geophysical Research: Atmospheres*, *115*(D12). https://doi.org/10.1029/2009JD013170

MacDougall, A. H., González-Rouco, J. F., Stevens, M. B., & Beltrami, H. (2008). Quantification of subsurface heat storage in a GCM simulation. *Geophysical Research Letters*, *35*(13). https://doi.org/10.1029/2008GL034639

Mankoff, K. D., Colgan, W., Solgaard, A., Karlsson, N. B., Ahlstrøm, A. P., van As, D., Box, J. E., Khan, S. A., Kjeldsen, K. K., Mouginot, J., & Fausto, R. S. (2019). Greenland Ice Sheet solid ice discharge from 1986 through 2017. *Earth Syst. Sci. Data*, *11*(2), 769–786. https://doi.org/10.5194/essd-11-769-2019

Marshall, J., Scott, J. R., Armour, K. C., Campin, J.-M., Kelley, M., & Romanou, A. (2015). The ocean's role in the transient response of climate to abrupt greenhouse gas forcing. *Climate Dynamics*, *44*(7), 2287–2299. https://doi.org/10.1007/s00382-014-2308-0

Marvel, K., Pincus, R., Schmidt, G. A., & Miller, R. L. (2018). Internal Variability and Disequilibrium Confound Estimates of Climate Sensitivity From Observations. *Geophysical Research Letters*, *45*(3), 1595–1601. https://doi.org/10.1002/2017GL076468

Marzeion, B., Leclercq, P. W., Cogley, J. G., & Jarosch, A. H. (2015). Brief Communication: Global reconstructions of glacier mass change during the 20th century are consistent. *The Cryosphere*, *9*(6), 2399–2404. https://doi.org/10.5194/tc-9-2399-2015

Matthews, T. K. R., Wilby, R. L., & Murphy, C. (2017). Communicating the deadly consequences of global

warming for human heat stress. *Proceedings of the National Academy of Sciences*, *114*(15), 3861. https://doi.org/10.1073/pnas.1617526114

Mayer, M., Fasullo, J. T., Trenberth, K. E., & Haimberger, L. (2016). ENSO-driven energy budget perturbations in observations and CMIP models. *Climate Dynamics*, *47*(12), 4009–4029. https://doi.org/10.1007/s00382-016-3057-z

Mayer, M., Haimberger, L., & Balmaseda, M. A. (2014). On the Energy Exchange between Tropical Ocean Basins Related to ENSO*. *Journal of Climate*, *27*(17), 6393–6403. https://doi.org/10.1175/JCLI-D-14-00123.1

Mayer, M., Haimberger, L., Edwards, J. M., & Hyder, P. (2017). Toward Consistent Diagnostics of the Coupled Atmosphere and Ocean Energy Budgets. *Journal of Climate*, *30*(22), 9225–9246. https://doi.org/10.1175/JCLI-D-17-0137.1

Mayer, M., Tietsche, S., Haimberger, L., Tsubouchi, T., Mayer, J., & Zuo, H. (2019). An Improved Estimate of the Coupled Arctic Energy Budget. *Journal of Climate*, *32*(22), 7915–7934. https://doi.org/10.1175/JCLI-D-19-0233.1

Mayer, M., Trenberth, K. E., Haimberger, L., & Fasullo, J. T. (2013). The Response of Tropical Atmospheric Energy Budgets to ENSO*. *Journal of Climate*, *26*(13), 4710–4724. https://doi.org/10.1175/JCLI-D-12-00681.1

McPherson, M., García-García, A., Cuesta-Valero Francisco, J., Beltrami, H., Hansen-Ketchum, P., MacDougall, D., & Ogden Nicholas, H. (2017). Expansion of the Lyme Disease Vector Ixodes Scapularis in Canada Inferred from CMIP5 Climate Projections. *Environmental Health Perspectives*, *125*(5), 057008. https://doi.org/10.1289/EHP57

Mears, C. A., & Wentz, F. J. (2009a). Construction of the Remote Sensing Systems V3.2 Atmospheric Temperature Records from the MSU and AMSU Microwave Sounders. *Journal of Atmospheric and Oceanic Technology*, *26*(6), 1040–1056. https://doi.org/10.1175/2008JTECHA1176.1

Mears, C. A., & Wentz, F. J. (2009b). Construction of the RSS V3.2 Lower-Tropospheric Temperature Dataset from the MSU and AMSU Microwave Sounders. *Journal of Atmospheric and Oceanic Technology*, *26*(8), 1493–1509. https://doi.org/10.1175/2009JTECHA1237.1

Mears, C. A., & Wentz, F. J. (2017). A Satellite-Derived Lower-Tropospheric Atmospheric Temperature Dataset Using an Optimized Adjustment for Diurnal Effects. *Journal of Climate*, *30*(19), 7695–7718. https://doi.org/10.1175/JCLI-D-16-0768.1

Melo-Aguilar, C., González-Rouco, J. F., García-Bustamante, E., Navarro-Montesinos, J., & Steinert, N. (2018). Influence of radiative forcing factors on ground–air temperature coupling during the last millennium: implications for borehole climatology. *Clim. Past*, *14*(11), 1583–1606. https://doi.org/10.5194/cp-14-1583-2018

Meyssignac, B., Boyer, T., Zhao, Z., Hakuba, M. Z., Landerer, F. W., Stammer, D., Köhl, A., Kato, S., L'Ecuyer, T., Ablain, M., Abraham, J. P., Blazquez, A., Cazenave, A., Church, J. A., Cowley, R., Cheng, L., Domingues, C. M., Giglio, D., Gouretski, V., … Zilberman, N. (2019). Measuring Global Ocean Heat Content to Estimate the Earth Energy Imbalance. *Frontiers in Marine Science*, *6*, 432. https://www.frontiersin.org/article/10.3389/fmars.2019.00432

Mouginot, J., Rignot, E., Bjørk, A. A., van den Broeke, M., Millan, R., Morlighem, M., Noël, B., Scheuchl, B., & Wood, M. (2019). Forty-six years of Greenland Ice Sheet mass balance from 1972 to 2018. *Proceedings of the National Academy of Sciences*, *116*(19), 9239. https://doi.org/10.1073/pnas.1904242116

Myhre, G., Shindell, D., Bréon, F.-M., Collins, W., Fuglestvedt, J., Huang, J., Koch, D., Lamarque, J.-F., Lee, D., Mendoza, B., Nakajima, T., Robock, A., Stephens, G., Takemura, T., & Zhang, H. (2013). Anthropogenic and natural radiative forcing. In *Climate Change 2013 the Physical Science Basis: Working Group I Contribution to the Fifth Assessment Report of the Intergovernmental Panel on Climate Change* (Vol. 9781107057, pp. 659–740). https://doi.org/10.1017/CBO9781107415324.018

Nauels, A., Meinshausen, M., Mengel, M., Lorbacher, K., & Wigley, T. M. L. (2017). Synthesizing long-term sea level rise projections – the MAGICC sea level model v2.0. *Geosci. Model Dev.*, *10*(6), 2495–2524. https://doi.org/10.5194/gmd-10-2495-2017

Noël, B., van de Berg, W. J., van Wessem, J. M., van Meijgaard, E., van As, D., Lenaerts, J. T. M., Lhermitte, S., Kuipers Munneke, P., Smeets, C. J. P. P., van Ulft, L. H., van de Wal, R. S. W., & van den Broeke, M. R. (2018). Modelling the climate and surface mass balance of polar ice sheets using RACMO2 – Part 1: Greenland (1958–2016). *The Cryosphere*, *12*(3), 811–831. https://doi.org/10.5194/tc-12-811-2018

Palmer, M D, & McNeall, D. J. (2014). Internal variability of Earth's energy budget simulated by CMIP5 climate models. *Environmental Research Letters*, *9*(3), 034016. https://doi.org/10.1088/1748-9326/9/3/034016

Palmer, M D, Roberts, C. D., Balmaseda, M., Chang, Y.-S., Chepurin, G., Ferry, N., Fujii, Y., Good, S. A.,

Guinehut, S., Haines, K., Hernandez, F., Köhl, A., Lee, T., Martin, M. J., Masina, S., Masuda, S., Peterson, K. A., Storto, A., Toyoda, T., … Xue, Y. (2017). Ocean heat content variability and change in an ensemble of ocean reanalyses. *Climate Dynamics*, *49*(3), 909–930. https://doi.org/10.1007/s00382-015-2801-0

Palmer, Matthew D, Durack, P. J., Chidichimo, M. P., Church, J. A., Cravatte, S., Hill, K., Johannessen, J. A., Karstensen, J., Lee, T., Legler, D., Mazloff, M., Oka, E., Purkey, S., Rabe, B., Sallée, J.-B., Sloyan, B. M., Speich, S., von Schuckmann, K., Willis, J., & Wijffels, S. (2019). Adequacy of the Ocean Observation System for Quantifying Regional Heat and Freshwater Storage and Change . In *Frontiers in Marine Science* (Vol. 6, p. 416). https://www.frontiersin.org/article/10.3389/fmars.2019.00416

Palmer, Matthew D, Harris, G. R., & Gregory, J. M. (2018). Extending CMIP5 projections of global mean temperature change and sea level rise due to thermal expansion using a physically-based emulator. *Environmental Research Letters*, *13*(8), 084003. https://doi.org/10.1088/1748-9326/aad2e4

Parkes, D., & Marzeion, B. (2018). Twentieth-century contribution to sea-level rise from uncharted glaciers. *Nature*, *563*(7732), 551–554. https://doi.org/10.1038/s41586-018-0687-9

Parkinson, C. L. (2019). A 40-y record reveals gradual Antarctic sea ice increases followed by decreases at rates far exceeding the rates seen in the Arctic. *Proceedings of the National Academy of Sciences*, *116*(29), 14414. https://doi.org/10.1073/pnas.1906556116

Peixoto, J. P., & Oort, A. H. (1992). *Physics of climate*. New York, NY (United States); American Institute of Physics. https://www.osti.gov/servlets/purl/7287064

Pickler, C., Fausto, E., Beltrami, H., Mareschal, jean-claude, Suárez, F., Chacon-Oecklers, A., Blin, N., Calderón, M., Montenegro, A., Harris, R., & Tassara, A. (2018). Recent climate variations in Chile: Constraints from borehole temperature profiles. *Climate of the Past*, *14*, 559–575. https://doi.org/10.5194/cp-14-559-2018

Pollack, H. N., & Smerdon, J. E. (2004). Borehole climate reconstructions: Spatial structure and hemispheric averages. *Journal of Geophysical Research: Atmospheres*, *109*(D11). https://doi.org/10.1029/2003JD004163

Polyakov, I. V, Pnyushkov, A. V, Alkire, M. B., Ashik, I. M., Baumann, T. M., Carmack, E. C., Goszczko, I., Guthrie, J., Ivanov, V. V, Kanzow, T., Krishfield, R., Kwok, R., Sundfjord, A., Morison, J., Rember, R., & Yulin, A. (2017). Greater role for Atlantic inflows on sea-ice loss in the Eurasian Basin of the Arctic Ocean. *Science*, *356*(6335), 285. https://doi.org/10.1126/science.aai8204

Pritchard, H. D., Ligtenberg, S. R. M., Fricker, H. A., Vaughan, D. G., van den Broeke, M. R., & Padman, L. (2012). Antarctic ice-sheet loss driven by basal melting of ice shelves. *Nature*, *484*(7395), 502–505. https://doi.org/10.1038/nature10968

Purkey, S. G., & Johnson, G. C. (2010). Warming of Global Abyssal and Deep Southern Ocean Waters between the 1990s and 2000s: Contributions to Global Heat and Sea Level Rise Budgets. *Journal of Climate*, *23*(23), 6336–6351. https://doi.org/10.1175/2010JCLI3682.1

Ramírez, F., Afán, I., Davis, L. S., & Chiaradia, A. (2017). Climate impacts on global hot spots of marine biodiversity. *Science Advances*, *3*(2), e1601198. https://doi.org/10.1126/sciadv.1601198

Rhein, M., Rintoul, S., Aoki, S., Campos, E., Chambers, D., Feely, R., Gulev, S., Johnson, G., Josey, S., Kostianoy, A., Mauritzen, C., Roemmich, D., Talley, L., & Wang, F. (2013). *Observations: Ocean. In: Climate Change 2013: The Physical Science Basis. Contribution of Working Group I to the Fifth Assessment Report of the Intergovernmental Panel on Climate Change]*.

Rhein, M, Rintoul, S., Aoki, S., Campos, E., Change, D. C.-C., & 2013, undefined. (n.d.). *Observations: ocean (Contribution of Working Group I to the Fifth Assessment Report of the Intergovernmental Panel on Climate Change)*.

Rhein, Monika, Steinfeldt, R., Huhn, O., Sültenfuß, J., & Breckenfelder, T. (2018). Greenland Submarine Melt Water Observed in the Labrador and Irminger Sea. *Geophysical Research Letters*, *45*(19), 10, 510–570, 578. https://doi.org/10.1029/2018GL079110

Richter-Menge, J., M.L. Druckenmiller, and M. Jeffries, Eds., 2019: Arctic Report Card, 2019. https://www.arctic.noaa.gov/Report-Card.

Rignot, E., Mouginot, J., Scheuchl, B., van den Broeke, M., van Wessem, M. J., & Morlighem, M. (2019). Four decades of Antarctic Ice Sheet mass balance from 1979–2017. *Proceedings of the National Academy of Sciences*, *116*(4), 1095. https://doi.org/10.1073/pnas.1812883116

Riser, S. C., Freeland, H. J., Roemmich, D., Wijffels, S., Troisi, A., Belbéoch, M., Gilbert, D., Xu, J., Pouliquen, S., Thresher, A., Le Traon, P.-Y., Maze, G., Klein, B., Ravichandran, M., Grant, F., Poulain, P.-M., Suga, T., Lim, B., Sterl, A., … Jayne, S. R. (2016). Fifteen years of ocean observations with the global Argo array. *Nature Climate Change*, *6*(2), 145–153. https://doi.org/10.1038/nclimate2872

Roemmich, D., & Gilson, J. (2009). The 2004–2008 mean and annual cycle of temperature, salinity, and steric height in the global ocean from the Argo Program. *Progress in Oceanography*, *82*(2), 81–100.

1641 https://doi.org/https://doi.org/10.1016/j.pocean.2009.03.004

1642 Roy, S., Harris, R. N., Rao, R. U. M., & Chapman, D. S. (2002). Climate change in India inferred from geothermal
1643  observations. *Journal of Geophysical Research: Solid Earth*, *107*(B7), ETG 5-1-ETG 5-16.
1644  https://doi.org/10.1029/2001JB000536

1645 Santer, B. D., Po-Chedley, S., Zelinka, M. D., Cvijanovic, I., Bonfils, C., Durack, P. J., Fu, Q., Kiehl, J., Mears, C.,
1646  Painter, J., Pallotta, G., Solomon, S., Wentz, F. J., & Zou, C.-Z. (2018). Human influence on the seasonal
1647  cycle of tropospheric temperature. *Science*, *361*(6399), eaas8806. https://doi.org/10.1126/science.aas8806

1648 Santer, B. D., Solomon, S., Wentz, F. J., Fu, Q., Po-Chedley, S., Mears, C., Painter, J. F., & Bonfils, C. (2017).
1649  Tropospheric Warming Over The Past Two Decades. *Scientific Reports*, *7*(1), 2336.
1650  https://doi.org/10.1038/s41598-017-02520-7

1651 Schweiger, A. J., Wood, K. R., & Zhang, J. (2019). Arctic Sea Ice Volume Variability over 1901–2010: A Model-
1652  Based Reconstruction. *Journal of Climate*, *32*(15), 4731–4752. https://doi.org/10.1175/JCLI-D-19-0008.1

1653 Schweiger, A., Lindsay, R., Zhang, J., Steele, M., Stern, H., & Kwok, R. (2011). Uncertainty in modeled Arctic sea
1654  ice volume. *Journal of Geophysical Research: Oceans*, *116*(C8). https://doi.org/10.1029/2011JC007084

1655 Seneviratne, S., Donat, M., Mueller, B., & Alexander, L. (2014). No pause in the increase of hot temperature
1656  extremes. *Nature Climate Change*, *4*. https://doi.org/10.1038/nclimate2145

1657 Seneviratne, S. I., Corti, T., Davin, E. L., Hirschi, M., Jaeger, E. B., Lehner, I., Orlowsky, B., & Teuling, A. J.
1658  (2010). Investigating soil moisture–climate interactions in a changing climate: A review. *Earth-Science
1659  Reviews*, *99*(3–4), 125–161. https://doi.org/10.1016/J.EARSCIREV.2010.02.004

1660 Seneviratne, S., Lüthi, D., Litschi, M., & Schär, C. (2006). Land-atmosphere coupling and climate change in
1661  Europe. *Nature*, *443*, 205–209. https://doi.org/10.1038/nature05095

1662 Serreze, M. C., & Barry, R. G. (2011). Processes and impacts of Arctic amplification: A research synthesis. *Global
1663  and Planetary Change*, *77*(1–2), 85–96. https://doi.org/10.1016/J.GLOPLACHA.2011.03.004

1664 Shepherd, A., Fricker, H. A., & Farrell, S. L. (2018). Trends and connections across the Antarctic cryosphere.
1665  *Nature*, *558*(7709), 223–232. https://doi.org/10.1038/s41586-018-0171-6

1666 Shepherd, A., Ivins, E., Rignot, E., Smith, B., van den Broeke, M., Velicogna, I., Whitehouse, P., Briggs, K.,
1667  Joughin, I., Krinner, G., Nowicki, S., Payne, T., Scambos, T., Schlegel, N., A, G., Agosta, C., Ahlstrøm, A.,
1668  Babonis, G., Barletta, V., … team, T. I. (2018). Mass balance of the Antarctic Ice Sheet from 1992 to 2017.
1669  *Nature*, *558*(7709), 219–222. https://doi.org/10.1038/s41586-018-0179-y

1670 Sherwood, S. C., & Huber, M. (2010). An adaptability limit to climate change due to heat stress. *Proceedings of the
1671  National Academy of Sciences*, *107*(21), 9552. https://doi.org/10.1073/pnas.0913352107

1672 Shi, J.-R., Xie, S.-P., & Talley, L. D. (2018). Evolving Relative Importance of the Southern Ocean and North
1673  Atlantic in Anthropogenic Ocean Heat Uptake. *Journal of Climate*, *31*(18), 7459–7479.
1674  https://doi.org/10.1175/JCLI-D-18-0170.1

1675 Smerdon, J. E., & Stieglitz, M. (2006). Simulating heat transport of harmonic temperature signals in the Earth's
1676  shallow subsurface: Lower-boundary sensitivities. *Geophysical Research Letters*, *33*(14).
1677  https://doi.org/10.1029/2006GL026816

1678 Steiner, A., Ladstädter, F., Randel, W. J., Maycock, A. C., Claud, C., Fu, Q., Gleisner, H., Haimberger, L., Ho, S.-
1679  P., Keckhut, P., Leblanc, T., Mears, C., Polvani, L., Santer, B., Schmidt, T., Sofieva, V., Wing, R., & Zou, C.-
1680  Z. (2020). Observed temperature changes in the troposphere and stratosphere from 1979 to 2018. *Journal of
1681  Climate*, https://doi.org/doi:10.1175/JCLI-D-19-0998.1

1682 Stevens, C. W. (2007). *Subsurface investigation of shallow-water permafrost located within the near-shore zone of
1683  the Mackenzie Delta, Northwest Territories, Canada*. University of Calgary.

1684 Stevens, M. B., González-Rouco, J. F., & Beltrami, H. (2008). North American climate of the last millennium:
1685  Underground temperatures and model comparison. *Journal of Geophysical Research: Earth Surface*, *113*(F1).
1686  https://doi.org/10.1029/2006JF000705

1687 Stieglitz, M., & Smerdon, J. E. (2007). Characterizing Land–Atmosphere Coupling and the Implications for
1688  Subsurface Thermodynamics. *Journal of Climate*, *20*(1), 21–37. https://doi.org/10.1175/JCLI3982.1

1689 Storto, A., Alvera-Azcárate, A., Balmaseda, M. A., Barth, A., Chevallier, M., Counillon, F., Domingues, C. M.,
1690  Drevillon, M., Drillet, Y., Forget, G., Garric, G., Haines, K., Hernandez, F., Iovino, D., Jackson, L. C.,
1691  Lellouche, J.-M., Masina, S., Mayer, M., Oke, P. R., … Zuo, H. (2019). Ocean Reanalyses: Recent Advances
1692  and Unsolved Challenges. *Frontiers in Marine Science*, *6*, 418. https://doi.org/10.3389/fmars.2019.00418

1693 Storto, A., Masina, S., Simoncelli, S., Iovino, D., Cipollone, A., Drevillon, M., Drillet, Y., Schuckman, K., Parent,
1694  L., Garric, G., Greiner, E., Desportes, C., Zuo, H., Balmaseda, M., & Peterson, K. (2018). The added value of
1695  the multi-system spread information for ocean heat content and steric sea level investigations in the CMEMS
1696  GREP ensemble reanalysis product. *Climate Dynamics*. https://doi.org/10.1007/s00382-018-4585-5

Straneo, F., Adusumilli, S., Slater, D., Timmermanns, M., Marzeion, B., & Schweiger, A. (2020). Inventory of Earth's ice loss and associated energy uptake from 1979 to 2017. *Geophysical Research Letters Letters*, *submitted*.

Straneo, Fiamma, & Cenedese, C. (2015). The Dynamics of Greenland's Glacial Fjords and Their Role in Climate. *Annual Review of Marine Science*, *7*(1), 89–112. https://doi.org/10.1146/annurev-marine-010213-135133

Suman, A., Dyer, F., & White, D. (2017). Late Holocene temperature variability in Tasmania inferred from borehole temperature data. *Clim. Past*, *13*(6), 559–572. https://doi.org/10.5194/cp-13-559-2017

Trenberth, K. E., Cheng, L., Jacobs, P., Zhang, Y., & Fasullo, J. (2018). Hurricane Harvey Links to Ocean Heat Content and Climate Change Adaptation. *Earth's Future*, *6*(5), 730–744. https://doi.org/10.1029/2018EF000825

Trenberth, K. E., & Fasullo, J. T. (2010). Tracking Earth's Energy. *Science*, *328*(5976), 316. https://doi.org/10.1126/science.1187272

Trenberth, K. E., & Fasullo, J. T. (2018). Applications of an Updated Atmospheric Energetics Formulation. *Journal of Climate*, *31*(16), 6263–6279. https://doi.org/10.1175/JCLI-D-17-0838.1

Trenberth, K. E., Fasullo, J. T., & Shepherd, T. G. (2015). Attribution of climate extreme events. *Nature Climate Change*, *5*(8), 725–730. https://doi.org/10.1038/nclimate2657

Trenberth, K. E., Fasullo, J. T., von Schuckmann, K., & Cheng, L. (2016). Insights into Earth's Energy Imbalance from Multiple Sources. *Journal of Climate*, *29*(20), 7495–7505. https://doi.org/10.1175/JCLI-D-16-0339.1

UN. (1992). *United Nations Framework Convention on Climate Change, FCCC/INFORMAL/84 GE.05-62220 (E) 200705*. https://unfccc.int/resource/docs/convkp/conveng.pdf

UN. (2015). *The Paris Agreement*. https://unfccc.int/sites/default/files/english_paris_agreement.pdf

UNGA. (2012). *The future we want, Resolution adopted by the General Assembly on 27 July 2012, A/RES/66/288*.

UNGA. (2015). *Transforming our world: the 2030 Agenda for Sustainable Development, Resolution adopted by the General Assembly on 25 September 2015, A/RES/70/1,*.

Vanderkelen, I., van Lipzig, N. P. M., Lawrence, D. M., Droppers, B., Golub, M., Gosling, S. N., Janssen, A. B. G., Marcé, R., Schmied, H. M., Perroud, M., Pierson, D., Pokhrel, Y., Satoh, Y., Schewe, J., Seneviratne, S. I., Stepanenko, V. M., Tan, Z., Woolway, R. I., & Thiery, W. (2020). Global Heat Uptake by Inland Waters. *Geophysical Research Letters*, *47*(12), e2020GL087867. https://doi.org/10.1029/2020GL087867

Vasseur, G., Bernard, P., Van de Meulebrouck, J., Kast, Y., & Jolivet, J. (1983). Holocene paleotemperatures deduced from geothermal measurements. *Palaeogeography, Palaeoclimatology, Palaeoecology*, *43*(3–4), 237–259. https://doi.org/10.1016/0031-0182(83)90013-5

Verdoya, M., Chiozzi, P., & Pasquale, V. (2007). Thermal log analysis for recognition of ground surface temperature change and water movements. *Clim. Past*, *3*(2), 315–324. https://doi.org/10.5194/cp-3-315-2007

von Schuckmann, K., Sallée, J.-B., Chambers, D., Le Traon, P.-Y., Cabanes, C., Gaillard, F., Speich, S., & Hamon, M. (2014). Consistency of the current global ocean observing systems from an Argo perspective. *Ocean Science*, *10*(3), 547–557. https://doi.org/10.5194/os-10-547-2014

von Schuckmann, K, & Le Traon, P.-Y. (2011). How well can we derive Global Ocean Indicators from Argo data? *Ocean Sci.*, *7*(6), 783–791. https://doi.org/10.5194/os-7-783-2011

von Schuckmann, K, Palmer, M. D., Trenberth, K. E., Cazenave, A., Chambers, D., Champollion, N., Hansen, J., Josey, S. A., Loeb, N., Mathieu, P.-P., Meyssignac, B., & Wild, M. (2016). An imperative to monitor Earth's energy imbalance. *Nature Climate Change*, *6*(2), 138–144. https://doi.org/10.1038/nclimate2876

von Schuckmann, Karina, Le Traon, P.-Y., Smith, N., Pascual, A., Brasseur, P., Fennel, K., Djavidnia, S., Aaboe, S., Fanjul, E. A., Autret, E., Axell, L., Aznar, R., Benincasa, M., Bentamy, A., Boberg, F., Bourdallé-Badie, R., Nardelli, B. B., Brando, V. E., Bricaud, C., … Zuo, H. (2018). Copernicus Marine Service Ocean State Report. *Journal of Operational Oceanography*, *11*(sup1), S1–S142. https://doi.org/10.1080/1755876X.2018.1489208

Wang, G., Cheng, L., Abraham, J., & Li, C. (2018). Consensuses and discrepancies of basin-scale ocean heat content changes in different ocean analyses. *Climate Dynamics*, *50*(7), 2471–2487. https://doi.org/10.1007/s00382-017-3751-5

Wang, X., Key, J., Kwok, R., & Zhang, J. (2016). Comparison of Arctic Sea Ice Thickness from Satellites, Aircraft, and PIOMAS Data. *Remote Sensing*, *8*(9), 713. https://doi.org/10.3390/rs8090713

Watts, N., Amann, M., Arnell, N., Ayeb-Karlsson, S., Belesova, K., Boykoff, M., Byass, P., Cai, W., Campbell-Lendrum, D., Capstick, S., Chambers, J., Dalin, C., Daly, M., Dasandi, N., Davies, M., Drummond, P., Dubrow, R., Ebi, K. L., Eckelman, M., … Montgomery, H. (2019). The 2019 report of The Lancet Countdown on health and climate change: ensuring that the health of a child born today is not defined by a changing climate. *The Lancet*, *394*(10211), 1836–1878. https://doi.org/10.1016/S0140-

6736(19)32596-6

WCRP, G. S. L. B. (2018). Global sea-level budget 1993–present. *Earth Syst. Sci. Data*, *10*(3), 1551–1590. https://doi.org/10.5194/essd-10-1551-2018

Wijffels, S., Roemmich, D., Monselesan, D., Church, J., & Gilson, J. (2016). Ocean temperatures chronicle the ongoing warming of Earth. In *Nature Climate Change* (Vol. 6, Issue 2, pp. 116–118). Nature Publishing Group. https://doi.org/10.1038/nclimate2924

Wild, M. (2020). The global energy balance as represented in CMIP6 climate models. *Climate Dynamics*. https://doi.org/10.1007/s00382-020-05282-7

Willis, J. K., Roemmich, D., & Cornuelle, B. (2004). Interannual variability in upper ocean heat content, temperature, and thermosteric expansion on global scales. *Journal of Geophysical Research: Oceans*, *109*(C12). https://doi.org/10.1029/2003JC002260

Wilson, N., Straneo, F., & Heimbach, P. (2017). Satellite-derived submarine melt rates and mass balance (2011–2015) for Greenland's largest remaining ice tongues. *The Cryosphere*, *11*, 2773–2782. https://doi.org/10.5194/tc-11-2773-2017

WMO. (2020). *WMO Statement on the State of the Global Climate in 2019*. https://library.wmo.int/doc_num.php?explnum_id=10211

Woollings, T., Gregory, J. M., Pinto, J. G., Reyers, M., & Brayshaw, D. J. (2012). Response of the North Atlantic storm track to climate change shaped by ocean–atmosphere coupling. *Nature Geoscience*, *5*(5), 313–317. https://doi.org/10.1038/ngeo1438

Xu, C., McDowell, N. G., Fisher, R. A., Wei, L., Sevanto, S., Christoffersen, B. O., Weng, E., & Middleton, R. S. (2019). Increasing impacts of extreme droughts on vegetation productivity under climate change. *Nature Climate Change*, *9*(12), 948–953. https://doi.org/10.1038/s41558-019-0630-6

Yang, H., Lohmann, G., Wei, W., Dima, M., Ionita, M., & Liu, J. (2016). Intensification and poleward shift of subtropical western boundary currents in a warming climate. *Journal of Geophysical Research: Oceans*, *121*(7), 4928–4945. https://doi.org/10.1002/2015JC011513

Zanna, L., Khatiwala, S., Gregory, J. M., Ison, J., & Heimbach, P. (2019). Global reconstruction of historical ocean heat storage and transport. *Proceedings of the National Academy of Sciences*, *116*(4), 1126. https://doi.org/10.1073/pnas.1808838115

Zemp, M., Huss, M., Thibert, E., Eckert, N., McNabb, R., Huber, J., Barandun, M., Machguth, H., Nussbaumer, S. U., Gärtner-Roer, I., Thomson, L., Paul, F., Maussion, F., Kutuzov, S., & Cogley, J. G. (2019). Global glacier mass changes and their contributions to sea-level rise from 1961 to 2016. *Nature*, *568*(7752), 382–386. https://doi.org/10.1038/s41586-019-1071-0

Zhang, J., & Rothrock, D. A. (2003). Modeling Global Sea Ice with a Thickness and Enthalpy Distribution Model in Generalized Curvilinear Coordinates. *Monthly Weather Review*, *131*(5), 845–861. https://doi.org/10.1175/1520-0493(2003)131<0845:MGSIWA>2.0.CO;2

Zscheischler, J., Westra, S., van den Hurk, B. J. J. M., Seneviratne, S. I., Ward, P. J., Pitman, A., AghaKouchak, A., Bresch, D. N., Leonard, M., Wahl, T., & Zhang, X. (2018). Future climate risk from compound events. *Nature Climate Change*, *8*(6), 469–477. https://doi.org/10.1038/s41558-018-0156-3